Protein Structure Tokenization via Geometric Byte Pair Encoding

Michael Sun[1,2]**, Weize Yuan**[3]**, Gang Liu**[4]**, Wojciech Matusik**[1]**, Marinka Zitnik**[2]
[1]MIT CSAIL   [2]Harvard Medical School   [3]Apple   [4]Notre Dame
{msun415,wojciech}@csail.mit.edu, marinka@hms.harvard.edu

Abstract

Protein structure is central to biological function, and enabling multimodal protein models requires joint reasoning over sequence, structure, and function. A key barrier is the lack of principled protein structure tokenizers (PSTs): existing approaches fix token size or rely on continuous vector codebooks, limiting interpretability, multi-scale control, and transfer across architectures. We introduce GEOBPE, a geometry-grounded PST that transforms continuous, noisy, multi-scale backbone conformations into discrete "sentences" of geometry while enforcing global constraints. Analogous to byte-pair encoding, GEOBPE generates a hierarchical vocabulary of geometric primitives by iteratively (i) clustering Geo-Pair occurrences with k-medoids to yield a resolution-controllable vocabulary; (ii) quantizing each Geo-Pair to its closest medoid prototype; and (iii) reducing drift through differentiable inverse kinematics that optimizes boundary glue angles under an $SE(3)$ end-frame loss. GEOBPE offers compression ($>10\times$ reduction in bits-per-residue at similar distortion rate), data efficiency ($>10\times$ less training data), and generalization (maintains test/train distortion ratio of $1.0 - 1.1$). It is architecture-agnostic: (a) its hierarchical vocabulary provides a strong inductive bias for coarsening residue-level embeddings from large PLMs into motif- and protein-level representations, consistently outperforming leading PSTs across 12 tasks and 24 test splits; (b) paired with a transformer, GEOBPE supports unconditional backbone generation via language modeling; and (c) tokens align with CATH functional families and support expert-interpretable case studies, offering functional meaning absent in prior PSTs. Code is available at https://github.com/shiningsunnyday/PT-BPE/.
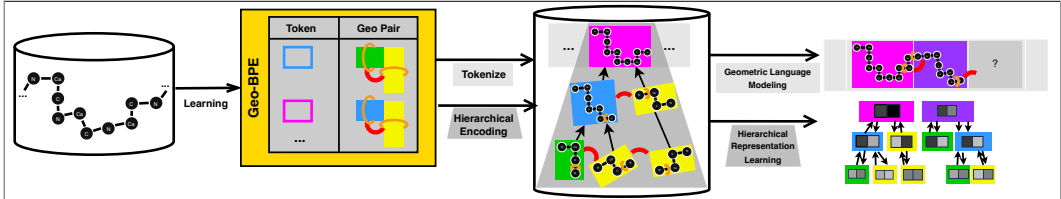
1 Introduction

Protein language models (PLMs) trained on large sequence databases capture evolutionary constraints (Rives et al., 2021) and support de novo sequence design (Lin et al., 2023b), but they do not explicitly model fold geometry and may underperform on tasks where function depends on structural interactions (Abramson et al., 2024; Gelman et al., 2025). In natural language processing, byte-pair encoding (BPE) constructs a vocabulary by iteratively merging the most frequent symbol pairs, producing a hierarchical representation of text (Larsson & Moffat, 2002). Despite BPE's success on sequential data, there is no geometric analog that can encode and decode protein backbone conformations. The central difficulty is discretizing continuous, noisy structural variability while preserving global consistency. Because protein folds are organized into modular substructures (Petsko & Ringe, 2004), a protein structure tokenizer should (a) build a hierarchical vocabulary of structural motifs and (b) segment folds into hierarchical decompositions, producing symbolic and interpretable representations of backbone geometry.

Recently, vector-quantized variational autoencoders (VQ-VAEs) have become the most popular class of protein structure tokenizers (PSTs), as adopted by ESM3 (Hayes et al., 2025) and others. VQ-VAEs learn an autoencoder that compresses and reconstructs a protein structure with N residues to and from N quantized latent codes, which are discrete "words" drawn from a vocabulary of learnable embeddings (Van Den Oord et al., 2017). While powerful, VQ-VAEs lack the efficiency, interpretability and modularity of BPE tokenizers: (1) using a fixed codebook can create performance bottlenecks and imbalance token usage frequency, handicapping downstream performance (Yuan et al., 2025); (2) using vectors as tokens over real data hinders interpretability, as rows of a

2D matrix do not capture the hierarchical relationships between sub-words like in BPE; (3) lastly, fixing all tokens to have the same size prevents multi-scale resolution, which is key to tasks that identify naturally occurring higher-level functional activity which span variable residue lengths.

Present work. We develop Geometric Byte-Pair Encoding (GEOBPE), a tokenizer that discretizes continuous protein backbones into symbolic "sentences" of structural motifs while learning a hierarchical vocabulary. The design is motivated by two requirements: (i) protein folds contain modular substructures that should be captured as reusable tokens, and (ii) discrete approximations must preserve global geometric consistency. To meet these requirements, GEOBPE alternates between local updates and global corrections. At each step, frequent motif pairs are clustered with k-medoids and replaced by representative prototypes, recursively building higher-order motifs. This local quantization inevitably introduces geometric drift, which GEOBPE corrects by optimizing boundary glue angles through differentiable inverse kinematics under an $SE(3)$ end-frame loss. The output after each iteration is a segmentation of the backbone into quantized motifs and glue parameters; the sequence of iterations yields a hierarchical decomposition of the fold, represented as a merge tree of structural motifs (Fig. 1). Our contributions are as follows: ① GEOBPE is the first geometry-grounded BPE analog for protein backbones, which builds a hierarchical vocabulary of motifs and tokenizes structures through an alternating global-local decomposition with glue-aware reconstruction. ② On benchmark datasets, GEOBPE traces a smooth Pareto front of compression-distortion tradeoffs, achieving up to 0.27-0.36× the bits-per-residue of ProToken and strong out-of-distribution generalization (test/train RMSD ratio 1.16-1.28 vs. 6.4× for VQ-VAE). It also matches downstream accuracy when trained on as little as 1% of the pretraining data. ③ Hierarchical vocabularies from GEOBPE improve representation quality on tasks such as binding site prediction and fold classification, and a transformer trained on its tokens enables unconditional backbone generation. ④ Tokens align with CATH domain annotations and are supported by expert case studies, providing functional protein insights and multi-resolution interpretability.

Figure 1: GEOBPE tokenizes a protein into discrete motifs linked by boundary glue angles and learns a hierarchical vocabulary of frequent structural primitives via k-medoids and recursively merging Geo-Pairs; at each step glue angles are optimized with differentiable inverse kinematics to preserve the global fold. Tokenization yields a merge tree that provides multi-resolution and interpretable representations of protein structure.

2 RELATED WORK

Protein Structural Alphabets. Structural alphabets approximate protein folds as successions of geometric motifs (Branden & Tooze, 2012). de Brevern et al. (2000) introduced 16 five–residue protein blocks from Protein Data Bank (PDB) structures, assigning fragments by RMSD. Later work showed that over 90% of residues can be covered by such alphabets (de Brevern et al., 2002) and analyzed their quality and specificity (de Brevern, 2005). Alphabet strings provide 1D encodings of 3D geometry, enabling the use of sequence alignment for fold analysis and prediction (Mahajan et al., 2015; Vetrivel et al., 2017). Camproux et al. (1999) proposed 12 building blocks via Hidden Markov Models (HMMs) and extended it to capture whole-protein conformational variability (Camproux et al., 2004). HMMs use inter-alpha-carbon distances within four residues as observed variables. Broader tertiary descriptors, such as inter-residue distances or moment invariants (Durairaj et al., 2020), capture non-contiguous context; Mackenzie (2016) found ∼600 motifs describe more than half of structural space ($39 \cdot 10^6$ conformations), indicating variability collapses into limited modes. Such descriptors extend to protein-level retrieval and classification (Durairaj et al., 2020; Van Kempen et al., 2024; Barrio-Hernandez et al., 2023). GEOBPE builds on these insights by treating structural motifs as extensible primitives and dynamically adjusting alphabet size and token resolution, unlike fixed structural alphabets.

Protein Structure Tokenizers. Modern PSTs, most notably VQ-VAEs, construct structural alphabets by training deep autoencoders with vectorized codebooks that map continuous structure to dis-

crete codes (Van Den Oord et al., 2017). Building on this idea, FoldSeek (Van Kempen et al., 2024) introduced 3Di alphabets (20 discrete codes learned with VQ-VAE) that compress local structural features for efficient search and homology detection. Subsequent works integrate 3Di alphabets with PLMs: Heinzinger et al. (2024) translate between 3Di and amino acid sequences; Su et al. (2023) define "3Di-residue" tokens and show pretraining with this vocabulary improves prediction; and Li et al. (2024) use disentangled attention to jointly model 3Di and residue tokens with a structure quantization module. End-to-end VQ-VAEs avoid predefined descriptors by training equivariant encoders and decoders to tokenize structure directly, achieving near-perfect reconstruction but at high computational cost. Large-scale efforts such as ESM3 (Hayes et al., 2025), trained on 236 million structures, highlight the central role of tokenizers in scaling multimodal PLMs. Recent work benchmarks tokenizer performance itself: AIDO.St and ProTokens show that stronger compression improves retrieval (Van Kempen et al., 2024; Zhang et al., 2024c) but reduces reconstruction quality, and both Zhang et al. (2024c) and Lin et al. (2023a) integrate tokenizers tightly with transformers. GEOBPE differs by using its hierarchical vocabulary as an inductive bias for representation learning and by supporting geometry-grounded language modeling without latent space vector quantization.

Byte-Pair Encoding for Biological Data. BPE underlies modern language models and has been applied to biological sequences with mixed outcomes. On genomes, BPE achieves superior compression and improves over k-mers in language models (Dotan et al., 2024; Zhou et al., 2023), though Nguyen et al. (2023) find the opposite using Hyena. For functional tasks, BPE often performs best (Dotan et al., 2024), while on nucleotide-resolution tasks it can underperform (Lindsey et al., 2025). These results indicate tokenizer utility depends on task scale and architecture, motivating GEOBPE's architecture-agnostic design and multi-scale resolution. Linguistic differences between text and biological sequences further complicate direct transfer: BPE tokens do not align with domain boundaries (Suyunu et al., 2024) or regulatory motifs (Lindsey et al., 2025). Other studies emphasize the importance of vocabulary design, reduced amino acid alphabets impair structure prediction (Ieremie et al., 2024), while BPE vocabularies of 50–200 tokens are often optimal for sequence tasks (Tan et al., 2024). Overall, existing tokenizers, including BPE, lack *versatility for protein structures*. GEOBPE extends BPE by grounding tokenization in geometry, exposing parameters for quantization, vocabulary, and efficiency, while uniquely providing fine-grained resolution control and a hierarchical motif vocabulary.

3 METHODS

We first establish backbone geometry notations in Sec. 3.1. Sec. 3.2 presents the GEOBPE algorithm, detailing its components for motif clustering, adaptive quantization, and glue-aware refinement. Finally, Sec. 3.3 formalizes the principles that an ideal protein structure tokenizer should satisfy and evaluates how GEOBPE meets them.

3.1 NOTATION & PRELIMINARIES

Global Backbone Formulation. Let a protein backbone $t^{(\tau)}$ with $N^{(\tau)}$ residues be represented by the Cartesian coordinates $\{(N_i, \mathrm{CA}_i, C_i) \in \mathbb{R}^{3\times3}\}_{i=1}^{N^{(\tau)}}$ of backbone atoms (oxygen and C_β omitted). Define bond lengths, bond angles, and dihedrals:

$$\ell_i^{N-CA} = \|N_i - \mathrm{CA}_i\|, \; \ell_i^{CA-C} = \|\mathrm{CA}_i - C_i\| \;;\; \ell_i^{C-N} = \|C_i - N_{i+1}\|.$$

$$\theta_i^{NCAC} = \angle(N_i, \mathrm{CA}_i, C_i) \,,\; \theta_i^{CACN} = \angle(\mathrm{CA}_i, C_i, N_{i+1}) \; \theta_i^{CNCA} = \angle(C_i, N_{i+1}, \mathrm{CA}_{i+1}).$$

$$\psi_i = \angle(N_i, \mathrm{CA}_i, C_i, N_{i+1}), \; \omega_i = \angle(\mathrm{CA}_i, C_i, N_{i+1}, \mathrm{CA}_{i+1}), \; \phi_i = \angle(C_i, N_{i+1}, \mathrm{CA}_{i+1}, C_{i+1}).$$

The full internal representation thus contains $3N^{(\tau)} - 1$ bond lengths, $3N^{(\tau)} - 2$ bond angles, and $3N^{(\tau)} - 3$ dihedrals and is invariant to any $g = (R, t) \in \mathrm{SE}(3)$.

Local Formulation (Bond–Residue). For residue i we define the *bond–residue* as the ordered triple $(N_i - \mathrm{CA}_i)$, $(\mathrm{CA}_i - C_i)$, $(C_i - N_{i+1})$ together with its internal angles. For $i < N^{(\tau)}$ this includes the lengths ℓ_i^{N-CA}, ℓ_i^{CA-C}, ℓ_i^{C-N}, the bond angles θ_i^{NCAC}, θ_i^{CACN}, and the peptide dihedral ψ_i about $CA_i - C_i$. For $i = N^{(\tau)}$, it includes only bond lengths $\ell_{N^{(\tau)}}^{N-CA}$, $\ell_{N^{(\tau)}}^{CA-C}$, and angle $\theta_{N^{(\tau)}}^{NCAC}$ (the $(C-N)$ bond, $\theta_{N^{(\tau)}}^{CACN}$, $\theta_{N^{(\tau)}}^{CNCA}$, and $\{\psi, \omega, \phi\}_{N^{(\tau)}}$ dihedrals are absent).

Glue Parameters Between Neighboring Bond–Residue. Neighboring bond–residues i and $i+1$ are connected by a set of *glue* angles that place the bonds of residue $i+1$ relative to residue i.

These are $\Gamma_i = \left\{ \theta_i^{CNCA}, \phi_i, \omega_i \right\}$, i.e., one bond angle θ_i^{CNCA} (to place N_{i+1}–CA_{i+1}) and two dihedrals ϕ_i and ω_i (to orient $CA_{i+1} - C_{i+1}$ and the peptide plane). We adopt (ω, ϕ) here to emphasize the two independent dihedral DOFs spanning the peptide and CA torsions.

Motif Formulation. A *bond–residue motif* $\mathcal{M}_{p:q}$ is a contiguous block of bond–residues $i = p, \ldots, q$ ($1 \leq p \leq q \leq N^{(\tau)}$). Its internal parameters comprise $\left\{ \ell_i^{N-CA}, \ell_i^{CA-C}, \ell_i^{C-N}, \theta_i^{NCAC}, \theta_i^{CACN}, \psi_i \right\}_{i=p}^{q}$ (with the obvious omissions at $i = q = N^{(\tau)}$) together with the internal glue angles $\{\Gamma_i\}_{i=p}^{q-1}$ that connect consecutive bond–residues inside the motif. The joined motif $\mathcal{M}_{p:r}$ requires the union of the internal parameters of $\mathcal{M}_{p:q}$ and $\mathcal{M}_{q+1:r}$, plus the *external* glue angles Γ_q connecting the last and first bond-residues of $\mathcal{M}_{p:q}$ and $\mathcal{M}_{q+1:r}$.

Entry/Exit Frames. For residue i, define $F_i = (R_i, t_i) \in SE(3)$ with origin $t_i = CA_i$ and axes chosen so that the x-axis points from CA_i toward the C_i, the y-axis is the normalized component of the $CA_i - N_i$ direction orthogonal to x, and the z-axis completes a right-handed triad.

Per-Link Transform. Define the transform between consecutive residue frames $G_i := F_{i+1} F_i^{-1} \in SE(3)$. By construction, G_i is a deterministic function of the internal coordinates local to the link $i \to i+1$, namely $G_i = g\left(\ell_i^{CA-C}, \ell_i^{C-N}, \ell_{i+1}^{N-CA}, \theta_i^{NCAC}, \theta_i^{CACN}, \theta_i^{CNCA}, \psi_i, \omega_i, \phi_{i+1} \right)$, and, in particular, depends on the *glue set* $\Gamma_i = \{\theta_i^{CNCA}, \phi_{i+1}, \omega_i\}$.

Entry/Exit Transforms. For a motif $\mathcal{M}_{p:q}$, define $F_{p:q}^{\text{entry}} := F_p, F_{p:q}^{\text{exit}} := F_q$. The *internal* entry→exit transform is $T_{p:q}^{\text{int}} = F_{p:q}^{\text{exit}} (F_{p:q}^{\text{entry}})^{-1} = (G_{q-1}) \cdots (G_p)$, which depends only on the internal coordinates of $\mathcal{M}_{p:q}$. The *external glue* transform between consecutive motifs $\mathcal{M}_{p:q}$ and $\mathcal{M}_{q+1:r}$ is precisely the boundary link $T_{q \to q+1}^{\text{glue}} = F_{q+1} F_q^{-1} = G_q$, and is parameterized by the glue set Γ_q (and the adjacent three bond lengths).

3.2 GEOBPE ALGORITHM

GEOBPE (Algo. 1) is organized around four components: (1) clustering motif occurrences into representative structural modes, (2) maintaining an ordered map to track frequent Geo-Pairs, (3) adaptively quantizing Geo-Pairs with controllable resolution, and (4) applying rigid-body refinement to enforce global geometric consistency.

(1) Extracting Dominant Modes from a Set of Motif Occurrences. The core subroutine invoked by GEOBPE is Algo. 6, which clusters a set of length L raw backbone fragments into K representative prototypes. This induces a hard quantization of the fragment space, since every possible occurrence is assigned to exactly one prototype. Because RMSD defines a metric over fragments, the clustering yields a Voronoi partition of this space. Importantly, the medoids are themselves observed fragments, so each quantized symbol retains a concrete structural interpretation: it represents the closest empirically observed conformation, providing a denoised approximation of local variability. Each time we quantize, we substitute every non-medoid occurrence by its assigned medoid, replacing all internal angles with the medoid's internal angles, making it an exact copy of that medoid (same length and per-position angles).

(2) Constructing a Structural Motif Alphabet. GEOBPE begins by quantizing all bond-residues and glue angles (Algo. 16) and building an *ordered* map (for dual-use as a *priority queue*, keyed by (occurrence count, grounding key)) of discrete geo-pair grounding keys to occurrences (Algo. 19). In each iteration (Algo. 9), GEOBPE pops the most frequent motif-pair key, runs Algo. 6 on all mapped occurrences, quantizes the occurrences, runs rigid-body refinement, and updates the dictionary to account for the new quantized backbone states.

(3) Multi-Resolution & Adaptive (Re-)Quantization. One-time quantization is a lossy procedure and is only needed to index Geo-Pairs occurrences in the current step. Thus, each GEOBPE iteration can re-quantize occurrences by referencing the original, even if prior iterations have quantized the same regions already. This allows resolution to adapt based on the size of the motif (e.g., coarse-grained for smaller motifs, fine-grained for larger ones), providing precise control over compression-reconstruction tradeoffs (see App. A).

(4) Minimizing Distortion via Rigid-Body Refinement. Let $T_{i:j}^{\text{int}}$ denote the entry→exit SE(3) map of a motif $\mathcal{M}_{i:j}$ determined by its internal coordinates. For an occurrence u with original motif $\mathcal{M}_{i_u:k_u}^{(t_u)}$, the rounding step replaces it by its assigned medoid segment:

$$\mathcal{M}_{i_u:k_u}^{(t_u)} \longrightarrow \mathcal{M}_{i_{\widehat{m}_c(u)}:k_{\widehat{m}_c(u)}}^{(t_{\widehat{m}_c(u)})},$$

4

Algorithm 1 GEOBPE: Protein structure tokenizer with geometric byte-pair encoding

---

Require: Backbones $\{t^{(1)}, \ldots, t^{(T)}\}$ with lengths $N^{(\tau)}$; residue codebook sizes (K_3, K_2); glue-IK
  weights (w_R, w_t); maximum merge iterations $S_{\max}$.
Ensure: Final vocabulary $\mathcal{V}$ (motif prototypes), final segmentations $\{\mathcal{P}^{(\tau)}\}$, final merge hierarchies
  $\{\mathcal{F}^{(\tau)}\}$, and the priority-ordered geo-pair map $\mathcal{D}$.
  1: **Empirical quantizer estimation (once).** Collect samples over all backbones for the 9 types
     $\{\ell^{N-CA}, \ell^{CA-C}, \ell^{C-N}\}, \{\theta^{NCAC}, \theta^{CACN}, \theta^{CNCA}\}, \{\phi, \psi, \omega\}$. Wrap angles to $[0, 2\pi)$ and build
     circular histograms with edges $0 = \beta_0 < \cdots < \beta_B = 2\pi$ that tile the circle; define Q by
     snapping to bin centers. For lengths, build linear histograms and snap to centers.
  2: **Per-residue initialization** (Algo. 16). Cluster interior and terminal bond–residues via
     RMSD_PARTITION to obtain codebooks $\mathcal{A}_3, \mathcal{A}_2$; overwrite each residue's internals by its as-
     signed prototype. Set the initial segmentation for each backbone:

$$\mathcal{P}^{(\tau)} = (\mathcal{M}_{1:1}^{(t_\tau)}, \ldots, \mathcal{M}_{N^{(\tau)}:N^{(\tau)}}^{(t_\tau)}).$$

Initialize hierarchies: for each τ, create a binary forest $\mathcal{F}^{(\tau)}$ whose leaves are the bond–residue
motifs $\mathcal{M}_{i:i}^{(t_\tau)}$, in order; its frontier equals $\mathcal{P}^{(\tau)}$. Initialize the vocabulary with base prototypes:

$$\mathcal{V} \leftarrow \{\text{residue-level keys} \mapsto \mathcal{A}_3, \mathcal{A}_2\}.$$

  3: **Global glue refinement** (Algo. 10). Optimize all boundary glues $\Gamma_i = \{\theta_i^{CNCA}, \omega_i, \phi_{i+1}\}$ via
     differentiable FK with (w_R, w_t); snap each to the nearest bin center using $Q_{\theta^{CNCA}}, Q_\omega, Q_\phi$.
  4: **Build the priority-ordered geo-pair map** (Algo. 19). Using the frontier leaves of each $\mathcal{F}^{(\tau)}$
     (equivalently, $\mathcal{P}^{(\tau)}$), construct the occurrence sets $\mathcal{O}(\kappa)$ and insert:

$$\mathcal{D}\big[(\rho(\kappa), -|\mathcal{O}(\kappa)|, \kappa)\big] \leftarrow \mathcal{O}(\kappa), \quad \rho(\kappa) = \mathbf{1}[\kappa \notin \mathrm{dom}(\mathcal{V})].$$

  5: **BPE loop – calls (Algo. 9) each step.**
  6: **for** $s = 1$ **to** $S_{\max}$ **do**
  7: $\quad (\{\mathcal{P}^{(\tau)}\}, \{\mathcal{F}^{(\tau)}\}, \mathcal{D}, \mathcal{V}) \leftarrow \mathrm{STEP}\big(\{\mathcal{P}^{(\tau)}\}, \{\mathcal{F}^{(\tau)}\}, \mathcal{D}, \mathcal{V}, \{Q_{\theta^{CNCA}}, Q_\omega, Q_\phi\}, (w_R, w_t)\big)$
  8: **end for**
  9: **return** $\mathcal{V}, \{\mathcal{P}^{(\tau)}\}, \{\mathcal{F}^{(\tau)}\}$, and $\mathcal{D}$.

---

where $\widehat{m}_{c(u)}$ is the medoid index returned by RMSD_PARTITION (an index into $\mathcal{S}$). Let $T_u^{\mathrm{occ}} :=$
$T_{i_u:k_u}^{\mathrm{int}}$ and $T_u^{\mathrm{med}} := T_{i_{\widehat{m}_{c(u)}}:k_{\widehat{m}_{c(u)}}}^{\mathrm{int}}$. Rounding thus replaces T_u^{occ} by T_u^{med}, and the induced
discrepancy $\Delta T_u := T_u^{\mathrm{occ}}\big(T_u^{\mathrm{med}}\big)^{-1}$ is the *drift* introduced by quantization. If left uncompensated,
products of such ΔT_u across a chain accumulate and move exit frames off their original targets. Each
boundary provides 3 *gluing* degrees of freedom (Γ_i) that can absorb this drift. To exactly recover the
original exit (in the idealized case), the boundary transform at the link $i_u - 1 \to i_u$ should satisfy:

$$\overbrace{G_{i_u-1}^{\mathrm{new}}}^{\text{opt vars}} T_u^{\mathrm{med}} \approx G_{i_u-1}^{\mathrm{orig}} T_u^{\mathrm{occ}} \qquad \Longrightarrow \qquad G_{i_u-1}^{\mathrm{new}} \approx G_{i_u-1}^{\mathrm{orig}} \Delta T_u,$$

where the quantization drift is $\Delta T_u := T_u^{\mathrm{occ}}\big(T_u^{\mathrm{med}}\big)^{-1}$. Since G_{i_u-1} is controlled by only three
gluing DOFs, we solve for $G_{i_u-1}^{\mathrm{new}}$ in least squares via the end-frame fitting objective:

$$\mathcal{L}_u(\Gamma_{i_u-1}) = w_R \big\| \log\big((\widehat{R}_{k_u})^\top R_{k_u}^\star\big)\big\|_2^2 + w_t \big\|\widehat{t}_{k_u} - t_{k_u}^\star\big\|_2^2,$$

with forward kinematics $\widehat{F}_{k_u} = F_{i_u-1}^\star G_{i_u-1}^{\mathrm{new}} T_u^{\mathrm{med}}, \quad F_{k_u}^\star = F_{i_u-1}^\star G_{i_u-1}^{\mathrm{orig}} T_u^{\mathrm{occ}}$. When
quantizing many motifs on the same backbone, performing this optimization each time can become
computationally prohibitive. Instead, we adopt a global (batch) alternative which treats all gluing
DOFs as parameters, with a global end-frame fitting loss. This provides maximum flexibility in drift
compensation. The algorithmic details are in Algo. 17 and 10.

Transferring Hierarchical Inductive Biases. GEOBPE can adapt the receptive field of a base
feature extractor Θ to that of the whole structure, supporting fine-grained embeddings for localized
predictions (e.g., active site prediction), coarse-grained embeddings for global predictions (e.g.,
fold classification), connecting both scales through recursive aggregation. Algo. 1 emits $\{\mathcal{F}^{(\tau)}\}$

as a forest, where leaf nodes represent residues and parent nodes represent motifs. Leaf nodes are initialized with pretrained features, then embeddings propagate up along the parent-child relations of $F^{(\tau)}$ until the forest roots; a final step aggregates the forest roots into a protein-level contextual embedding; then they are propagated down until the leaf nodes; the final embeddings are output as vocabulary-induced features. See Algo. 13 for details.

3.3 PRINCIPLES OF PROTEIN STRUCTURE TOKENIZATION

Let $\mathcal{X} = (\mathbb{R}^{3 \times 3})^*$ be the space of backbone coordinate tensors and let $\mathcal{V}$ be a finite codebook. A tokenizer is a tuple $\mathsf{T} = (\mathcal{V}, \mathrm{Enc}, \mathrm{Dec})$: $\mathrm{Enc} : \mathcal{X} \to \mathcal{V}^*$ mapping a structure $\mathbf{x}$ to a finite token sequence $\mathbf{q} = \mathrm{Enc}(\mathbf{x})$, $\mathrm{Dec} : \mathrm{Im}(\mathrm{Enc}) \to \mathcal{X}$ mapping $\tilde{\mathbf{x}} = \mathrm{Dec}(\mathrm{Enc}(\mathbf{x}))$. For dataset $\mathcal{D} \subset \mathcal{X}$ and distortion $d : \mathcal{X} \times \mathcal{X} \to [0, \infty)$ (e.g., Kabsch-aligned RMSD per residue), define:

$$\Delta(\mathsf{T}; \mathcal{D}) = \frac{1}{|\mathcal{D}|} \sum_{\mathbf{x} \in \mathcal{D}} d(\mathbf{x}, \mathrm{Dec}(\mathrm{Enc}(\mathbf{x}))), \qquad \mathrm{BPR}(\mathsf{T}; \mathcal{D}) = \frac{\mathrm{L}(\mathsf{T}) + \sum_{\mathbf{x} \in \mathcal{D}} \mathrm{L}(\mathrm{Enc}(\mathbf{x}))}{\sum_{\mathbf{x} \in \mathcal{D}} N(\mathbf{x})} \text{ bits/res}$$

where $\mathrm{L}(\mathsf{T}) \geq 0$ is the description length of $(\mathcal{V}, \mathrm{Enc}, \mathrm{Dec})$ and $N(\mathbf{x})$ is the residue count; under a uniform per-token code, $\mathrm{L}(\mathrm{Enc}(\mathbf{x})) = |\mathrm{Enc}(\mathbf{x})| \log_2 |\mathcal{V}|$. We setup the following principles for an ideal tokenizer $\widehat{\mathsf{T}}$ and empirically explore the degree GEOBPE satisfies them.

Principle 1: Pareto-optimal on $\mathcal{D}$. $\widehat{\mathsf{T}}$ is Pareto-optimal on $\mathcal{D}$ iff no T' satisfies $\mathrm{BPR}(\mathsf{T}'; \mathcal{D}) \leq \mathrm{BPR}(\widehat{\mathsf{T}}; \mathcal{D})$ and $\Delta(\mathsf{T}'; \mathcal{D}) \leq \Delta(\widehat{\mathsf{T}}; \mathcal{D})$, with at least one strict. We empirically explore this principle by evaluating Pareto-efficiency among leading PSTs and codebook configurations in Fig. 3.

Priciple 2: Out-of-distribution (OOD) generalization. $\widehat{\mathsf{T}}$ generalizes OOD if, on unseen test set $\mathcal{D}_{\text{test}} \subset \mathcal{X}, \Delta(\mathsf{T}; \mathcal{D}_{\text{test}}) \approx \Delta(\mathsf{T}; \mathcal{D})$. We depict generalization gaps of leading PSTs in Fig. 3.

Principle 3: Downstream transfer via codebook/vocabulary. Let $\mathcal{V}$ be the vocabulary of T and let $N(\mathbf{x})$ be the residue count. Let Θ parameterize a pretrained feature extractor. The codebook/vocabulary $\mathcal{V}$ *induces* per-residue features $r_{\mathcal{V}}(\mathbf{x}) = \Psi_{\mathcal{V}}(F_{\Theta}(\mathbf{x})) \in (\mathbb{R}^d)^{N(\mathbf{x})}$. An ideal tokenizer of protein *structures* should go beyond pure compression; it should learn useful signals related to function. We loosely define the ability of a PST to transfer useful signals by test performance on a battery of downstream tasks when parameterizing samples $\mathbf{x}$ by the vocabulary $\mathcal{V}$ together with a feature extractor Θ. We benchmark downstream transfer of GEOBPE against others in Table 1.
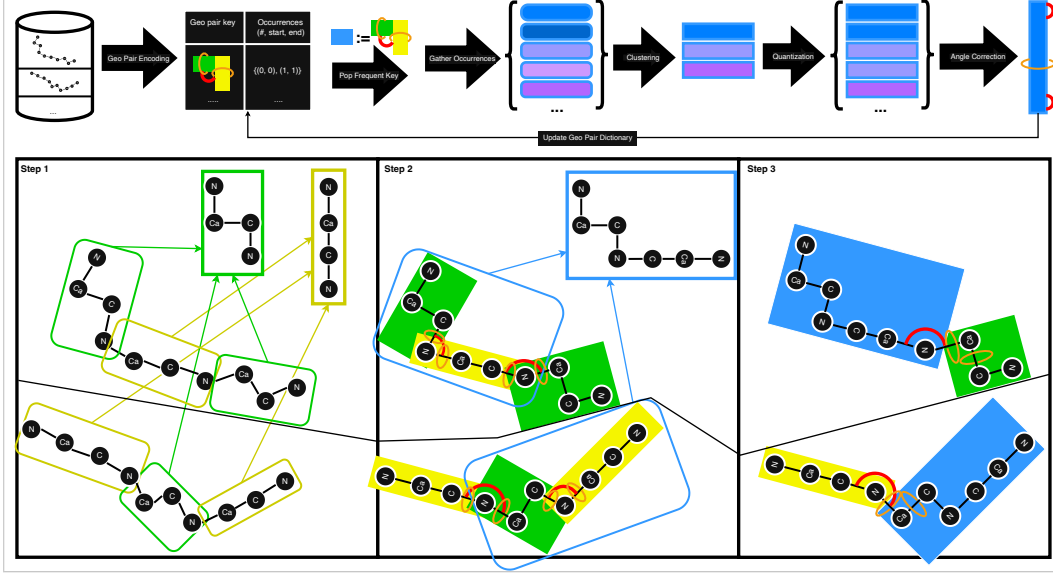
4 EXPERIMENTS

We answer ten research questions (Q1-Q10) to benchmark the performance, efficiency, and application integration potential of GEOBPE against other popular tokenizers.

- **Tokenization Performance**: (Q1) How many bits are needed to store the tokenizer and tokenized inputs? (Q2) How faithful is the reconstruction? (Q3) How does performance generalize to unseen data? (Q4) How many samples are needed to train the tokenizer?
- **Token Efficiency**: (Q5) How frequent and balanced is vocabulary utilization? (Q6) Does small-scale autoregressive token modeling generate reasonable designs?
- **Downstream Transfer**: (Q7) How much transferrable signal does the tokenizer capture about the data? (Q8) How much does the vocabulary help on representation learning tasks?
- **Interpretability**: (Q9) How well do GEOBPE tokens agree with "ground-truth" domain annotations? (Q10) Can experts *understand* GEOBPE through real-world case studies?

Datasets. We follow the same dataset splits as in Yuan et al. (2025). Pretraining uses structures from the Protein Data Bank following OpenFold2's protocol and retained a non-redundant subset of $\approx$48K protein chains, which were split into training/validation sets, with CAMEO and CASP14 reserved as held-out test sets for evaluating OOD generalization and token efficiency. For downstream evaluation, we use 8 datasets, spanning residue-level classification (ligand binding, catalytic, conserved, repeat, and epitope), residue-level regression (structural flexibility prediction), and protein-level classification. Together these datasets probe functional relevance, structural variability, token distinctiveness, and efficiency across a wide range of proteins. For citations and details, see App. B.

Baselines. We compare with VQ-VAEs, the leading family of discrete PSTs (Hayes et al., 2025; Van Kempen et al., 2024; Lin et al., 2023a; Yuan et al., 2025). They consist of (1) a structure encoder maps structure $\boldsymbol{x}$ into a continuous representation $z \in \mathbb{R}^{N \times D}$; (2) a vector quantization layer

Figure 2: (Top) GeoBPE tracks a Geo-Pair Encoding, a dictionary mapping Geo-Pair keys to occurrences at all times. Each step pops the most frequent Geo-Pair key, gathers the occurrences and selects K prototypes to add to $\mathcal{V}$. All occurrences are quantized to the closest prototype. Glue angles are optimized to correct for the drift introduced. (Bottom) Toy example with two backbones; we initialize residue-orientation modes using two prototypes (green & yellow), pop the frequent Geo-Pair (blue), quantize occurrences (rounded → sharp corners), and optimize glue angles (red and orange).

discretizes each z_i by selecting $k_i = \arg\min_j d(z_i, q_j)$ from a learnable codebook $Q \in \mathbb{R}^{K \times D}$; and (3) a structure decoder reconstructs $\tilde{x} \approx x$ from the discrete codes $q_k = \{q_{k_j}\}_{j=1}^L$. We also compare with Inverse Folding (IF) *continuous* PSTs, which skips the quantization step $z \to q_k$ and trained to recover the amino acid sequence from z (Dauparas et al., 2022; Yang et al., 2023).
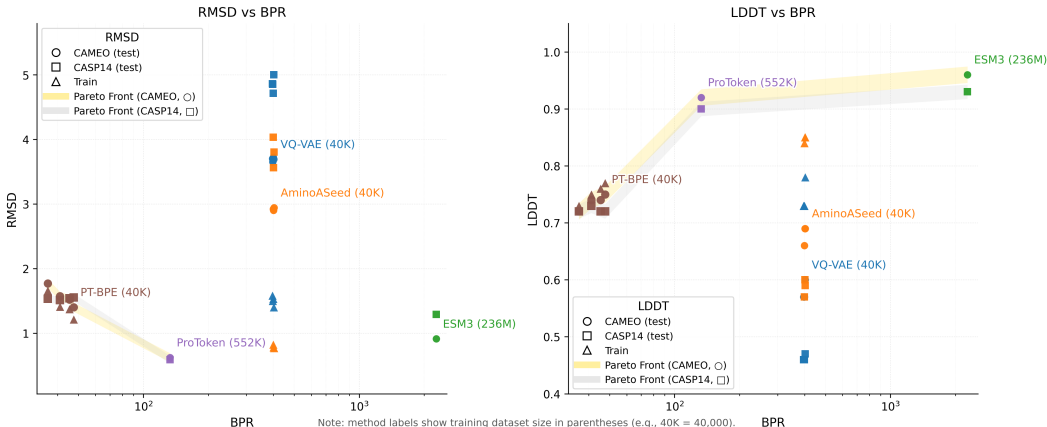
Downstream Transfer. For VQ-VAEs, Θ and $\mathcal{V}$ are *jointly* learned, so we set $r_\mathcal{V}^{\text{VQ-VAE}}(x) := r^{\text{VQ-VAE}}(x) \leftarrow \text{Enc}(x)$. For GEOBPE, we use $\Theta \leftarrow$ ESM3 to demonstrate how $\mathcal{V}^{\text{GEOBPE}}$ can transfer useful signals from $\mathcal{F}_\Theta(x)$ to $r_\mathcal{V}(\mathcal{F}_\Theta(x))$.

Performance Metrics. *Compression* measures Bits-Per-Residue (BPR), as defined in Sec. 3.3. *Distortion* (Δ) use standard RMSD and LDDT. *Token Efficiency* uses Codebook Utility Rate (UR), Perplexity (details in App. D) and *Small Structure Language Model Evaluation (SSLM-Eval)* (details in App. E). SSLM-Eval trains a small decoder-only Transformer on the same pretraining corpus *post*-tokenization (Algo. 2), then generates new sentences, detokenizes them into structures, and assesses generation results (Algo. 3, 4, 5). *Downstream Transfer* covers 12 tasks (24 test splits) using AUROC (%) for functional site prediction, Spearman's ρ (%) for flexibility prediction, and Macro F1 (%) for fold classification. *Expert Agreement* measures Domain & Segment Recall/Precision/F1/IOU (details in App. F).

Computational Complexity / Implementation Details. We analyze the theoretical complexity of GEOBPE in App. H and justify the steps we took towards efficient implementation and use.

5 RESULTS

Tokenizer Performance. We find GEOBPE and ProToken form the Pareto front under both $\Delta \in \{\text{RMSD}, \text{LDDT}\}$. GEOBPE achieves $0.271 - 0.358$x and $0.016 - 0.021$x the BPR of ProToken and ESM3, dropping LDDT by only $18 - 22\%$ and $22 - 25\%$, which are impressive feats considering GEOBPE's training data was only $\approx 7\%$ and 0.02% the size. We also observe GEOBPE's strong OOD generalization, with test/train RMSD peaking at 1.16 (CAMEO) and 1.28 (CASP), showing negligible degradation reconstructing unseen data; VQ-VAE/AminoASeed, using identical data splits, show degradation as high as 6.4x test RMSD. Crucially, as the GEOBPE codebook grows, the variants trace a near-linear path along the Pareto front toward ProToken, elastically trading off BPR for lower distortion, a feature other tokenizers do not have (as codebook dimensions are fixed).

Figure 3: Plots of $(\mathrm{BPR}(\mathsf{T};\mathcal{D}),\ \Delta(\mathsf{T};\mathcal{D}_{\mathrm{test}}))$ across tokenizers for $\Delta \in \{\mathrm{RMSD}, \mathrm{LDDT}\}$. We vary $|\mathcal{V}| \in \{128, 256, 512, 1024\}$ for VQ-VAE/AminoASeed and $|\mathcal{V}| \in \{600, 2500, 6000, 21000\}$ for GEOBPE to sample multiple points; we observe GEOBPE sweeps a smooth tradeoff curve.

Token Efficiency. We report UR & Perplexity averaged over held-out test sets to gauge code-book/vocabulary usage on unseen data, the setting where the tokenizer is deployed. In Table 6, we see all methods except VQ-VAE and ESM3 achieve an average UR of $> 40\%$; all except VQ-VAE achieve 0.2 average Perplexity. An ideal tokenizer avoids codebook collapse, but exactly uniform token usage may not be desirable. We introduce SSLM-Eval to stress test whether codebook efficiency actually leads to generative efficiency. SSLM-Eval is a holistic way to compare tokenizers using both encoder token efficiency *and* decoder's generative efficiency. In Table 7, we find GEOBPE is capable of generating 99% unique and designable backbones, achieving up to 49% higher scTM and maintaining higher diversity than both VQ-VAE methods using the same data splits. We visualize some realistic, novel backbones GEOBPE generated in App. E.4. Interestingly, the "less-efficient" VQ-VAE generated 58% more diverse backbones, demonstrating uniform token usage can be counterproductive to language modeling.

Downstream Task Transfer. In Table 1, we see GEOBPE-induced features rank first, on average, across both function and structure property prediction tasks. The relative performance gaps 15.44% and 43.28% quantify the add-on benefits of GEOBPE-induced features. GEOBPE-induced features reverse the trend that discrete PSTs produce less informative representations for downstream tasks (due to quantization-related issues (Yuan et al., 2025)), highlighting that *hierarchical structure* from discrete vocabularies raises the ceiling on downstream transfer. We include a series of further abla-tion studies in App. A, where key findings include (1) GEOBPE shows no drop in performance when using only 1% of the pretraining data (all hyperparameters held constant); (2) GEOBPE task-specific oracle tokenizers also show no drop in performance.

6 DISCUSSION

Case Study: Agreement with PFAM Annotations. We ran CATH Functional Families (FunFams) (Das et al., 2015b) to obtain domain boundaries and compared them against GEOBPE-derived mo-tifs. Because sequence conservation is linked to structural preservation, we expect overlap between predicted motifs and functional domains. In Table 2, GEOBPE achieves 99.97% domain recall with mean F1 = 0.996 and IOU = 0.992, showing near-perfect agreement across 10 datasets. *The agreement is not only geometric but also functional:* GEOBPE tokens frequently coincide with boundaries of ligand-binding grooves, transmembrane cavities, and scaffolding helices, capturing motifs that underlie molecular recognition and catalysis. This suggests GEOBPE does more than segment folds consistently: it surfaces interpretable structural primitives that map onto biochemical roles, offering a functional vocabulary absent in prior PSTs. Details are in App. F

Case Study: Human Expert Analysis of Interpretability. We conducted three expert evaluations of GEOBPE-derived hierarchies (App. G). Across proteins, the discovered motifs align with func-tionally meaningful substructures, including regions mediating ligand binding, molecular recogni-tion, and structural gating. In the SLC25A20 transporter (Fig. 8), GEOBPE isolates a transmem-brane binding cavity formed by helices and polar residues. In the 14-3-3:Tau complex (Fig. 9), it

Table 1: Downstream transfer performance benchmark. The relative performance v.s. ESM3 for GEOBPE is included. We underline and **bold** the best continuous and discrete PSTs, respectively; ▭ indicates the best method across both continuous and discrete PSTs. Omitted rows are in Table 4.

Task	Split	Continuous PST		Discrete PST					
		ProteinMPNN	MIF	FoldSeek	ProTokens	ESM3	VanillaVQ	AminoAseed	GEOBPE (v.s. ESM3)
					Functional Site Prediction (AUROC%)				
BindInt	Fold	51.83	50.38	53.18	44.66	44.30	47.25	47.11	**59.19 (+33.61%)**
	SupFam	94.00	94.56	46.26	86.05	90.77	86.71	90.53	**91.31 (+0.59%)**
BindBio	Fold	78.42	85.79	32.37	58.47	62.84	62.02	65.73	**94.94 (+51.08%)**
	SupFam	81.00	87.27	52.44	60.47	65.22	62.92	68.30	**95.94 (+47.10%)**
BindShake	Org	75.52	79.90	53.43	59.10	66.10	67.04	69.61	**87.73 (+32.72%)**
CatInt	Fold	61.05	59.62	53.43	58.16	61.09	58.89	62.19	**66.21 (+8.38%)**
	SupFam	93.40	96.49	51.41	83.85	89.82	85.00	**91.91**	88.65 (-1.30%)
CatBio	Fold	82.49	85.85	56.33	67.68	65.33	67.58	65.95	**95.01 (+45.43%)**
	SupFam	93.19	96.97	53.78	64.05	74.65	70.92	87.59	**95.90 +28.47%**
Con	Fold	57.18	58.43	49.20	57.20	55.22	56.98	57.23	**71.96 (+30.32%)**
	SupFam	84.68	92.66	51.31	70.64	80.53	74.60	**86.60**	84.84 (+5.35%)
				...2 tasks omitted (Rep, Ept)...					
Average AUROC%		75.92	79.82	51.90	65.37	69.24	68.30	72.43	79.93 (+15.44%)
					Physicochemical Property Prediction (Spearman's ρ%)				
FlexRMSF	Fold	62.37	59.60	15.35	13.81	44.53	44.22	**44.63**	40.89 (-8.17%)
	SupFam	59.24	56.80	11.99	7.62	39.08	38.98	40.99	**47.17 (20.70%)**
				...2 tasks omitted (FlexBFactor, FlexNEQ)...					
Average ρ%		54.41	52.73	7.80	9.84	37.35	33.49	38.08	45.26 (+21.18%)
					Structure Property Prediction (Macro F1%)				
Homo	Fold	25.66	22.56	11.57	5.84	**30.02**	18.17	29.87	23.60 (-21.39%)
	SupFam	30.83	33.86	4.67	6.17	24.89	22.10	38.38	**47.28 (+89.96%)**
	Fam	63.33	74.22	15.34	18.33	54.42	47.18	69.78	**85.75 (+57.47%)**
Average Macro F1%		39.94	43.55	10.51	10.11	36.44	29.15	46.01	52.21 (+43.28%)

Table 2: We annotate 100 PDBs from each dataset and report % of 1,000 random equal-length segmentations that GEOBPE matches or outscores. Omitted columns are in Table 5.

		BindInt	BindBio	BindShake	CatInt	CatBio	Con		Average
Domain	Mean Recall	99.95 (98.35)	100 (100.0)	100 (100.0)	100 (100.0)	99.99 (93.55)	99.95 (98.0)	*4 columns omitted*	99.97 (97.97)
	Mean Precision	98.9 (53.87)	99.62 (71.92)	99.76 (68.24)	99.28 (50.49)	99.33 (42.78)	99.19 (63.89)		99.25 (54.59)
	Mean F1	99.42 (86.48)	99.81 (83.63)	99.88 (76.49)	99.64 (62.56)	99.66 (61.04)	99.57 (87.03)		99.61 (76.82)
	Mean IOU	98.86 (86.32)	99.62 (83.63)	99.76 (76.54)	99.28 (62.44)	99.32 (60.94)	99.14 (86.97)	*... ...*	99.22 (76.75)
Segment	Mean Recall	100 (100.0)	100 (100.0)	100 (100.0)	100 (100.0)	100 (100.0)	100 (100.0)		100.00 (100.00)
	Mean Precision	97.16 (72.04)	81.84 (61.82)	97.64 (68.33)	90.4 (63.09)	98.87 (74.76)	98.92 (92.0)		95.11 (65.62)
	Mean F1	98.54 (72.04)	89.05 (61.82)	98.8 (68.33)	94.04 (63.09)	99.43 (74.76)	99.45 (92.0)		97.23 (65.62)

identifies a canonical phospho-binding groove stabilized by charged side chains. Recurrent local motifs (aromatic cages, polar bridges, helix-helix clamps) are combined into higher-order scaffolds that mirror established biochemical organization. *These hierarchies capture geometric regularities and also modular design principles conserved across folds and families.* Even in compact domains, such as nucleotide-recognition modules, GEOBPE motifs reveal the coupling between geometric curvature and chemical specificity, meaning that GEOBPE surfaces reusable motifs that are both interpretable and evolutionarily grounded.

Limitations. GEOBPE currently does not incorporate sequence or side chains, and $\mathcal{V}$-induced features remain dependent on pretrained PLMs. While we tested vocabularies up to 21K tokens, scalability to even larger codebooks and the associated computational tradeoffs remain open questions. The present generative integration is limited to a small-scale proof of concept, and extending it to more powerful models will require further development. Future work should also investigate incorporating side-chain geometry to capture finer-grained biochemical interactions.

7 CONCLUSION

We present GEOBPE, a principled geometry-grounded analog of BPE for protein folds. GEOBPE (a) captures natural conformational variability in protein backbones, (b) constructs a hierarchical vocabulary of structural motifs, and (c) produces hierarchical views of folds for downstream representation learning. Its hierarchies reveal conserved modular design principles that connect structure to function. Empirically, GEOBPE advances the state of the art in tokenizer performance, out-of-distribution generalization, token and generative efficiency, downstream transfer, and interpretability. These results establish GEOBPE as a foundation for structure-native protein language models.

8 REPRODUCIBILITY STATEMENT

We have included detailed descriptions of our method in the main text, to the extent we believe is sufficient to reproduce our method. In App. K, we include mathematical descriptions and algorithm pseudocodes for all mentioned algorithms and subroutines of a non-trivial nature. In App. I, we list the key hyperparameters, their effects on algorithm behavior, and the default values used in our experiments. We also note any deviations from the default values used to obtain the results reported in the main text. In App. H, we analyze the computational complexity of our method; we also describe practical implementation choices used to make the method efficient in practice.

REFERENCES

Josh Abramson, Jonas Adler, Jack Dunger, Richard Evans, Tim Green, Alexander Pritzel, Olaf Ronneberger, Lindsay Willmore, Andrew J Ballard, Joshua Bambrick, et al. Accurate structure prediction of biomolecular interactions with alphafold 3. *Nature*, 630(8016):493–500, 2024.

Gustaf Ahdritz, Nazim Bouatta, Christina Floristean, Sachin Kadyan, Qinghui Xia, William Gerecke, Timothy J O'Donnell, Daniel Berenberg, Ian Fisk, Niccolò Zanichelli, et al. Openfold: Retraining alphafold2 yields new insights into its learning mechanisms and capacity for generalization. *Nature methods*, 21(8):1514–1524, 2024.

Inigo Barrio-Hernandez, Jingi Yeo, Jürgen Jänes, Milot Mirdita, Cameron LM Gilchrist, Tanita Wein, Mihaly Varadi, Sameer Velankar, Pedro Beltrao, and Martin Steinegger. Clustering predicted structures at the scale of the known protein universe. *Nature*, 622(7983):637–645, 2023.

Matthias Blum, Antonina Andreeva, Laise Cavalcanti Florentino, Sara Rocio Chuguransky, Tiago Grego, Emma Hobbs, Beatriz Lazaro Pinto, Ailsa Orr, Typhaine Paysan-Lafosse, Irina Ponamareva, et al. Interpro: the protein sequence classification resource in 2025¡? mode longmeta?¿. *Nucleic acids research*, 53(D1):D444–D456, 2025.

Carl Ivar Branden and John Tooze. *Introduction to protein structure*. Garland Science, 2012.

AC Camproux, P Tuffery, JP Chevrolat, JF Boisvieux, and S Hazout. Hidden markov model approach for identifying the modular framework of the protein backbone. *Protein engineering*, 12 (12):1063–1073, 1999.

Anne-Cloude Camproux, Romain Gautier, and Pierre Tuffery. A hidden markov model derived structural alphabet for proteins. *Journal of molecular biology*, 339(3):591–605, 2004.

Henriette Capel, Robin Weiler, Maurits Dijkstra, Reinier Vleugels, Peter Bloem, and K Anton Feenstra. Proteinglue multi-task benchmark suite for self-supervised protein modeling. *Scientific Reports*, 12(1):16047, 2022.

Sayoni Das, David Lee, Ian Sillitoe, Natalie L Dawson, Jonathan G Lees, and Christine A Orengo. Functional classification of cath superfamilies: a domain-based approach for protein function annotation. *Bioinformatics*, 31(21):3460–3467, 2015a.

Sayoni Das, Ian Sillitoe, David Lee, Jonathan G Lees, Natalie L Dawson, John Ward, and Christine A Orengo. Cath funfhmmer web server: protein functional annotations using functional family assignments. *Nucleic acids research*, 43(W1):W148–W153, 2015b.

Justas Dauparas, Ivan Anishchenko, Nathaniel Bennett, Hua Bai, Robert J Ragotte, Lukas F Milles, Basile IM Wicky, Alexis Courbet, Rob J de Haas, Neville Bethel, et al. Robust deep learning–based protein sequence design using proteinmpnn. *Science*, 378(6615):49–56, 2022.

Alexandre G de Brevern. New assessment of a structural alphabet. *In silico biology*, 5(3):283–289, 2005.

Alexandre G de Brevern, Catherine Etchebest, and Serge Hazout. Bayesian probabilistic approach for predicting backbone structures in terms of protein blocks. *Proteins: Structure, Function, and Bioinformatics*, 41(3):271–287, 2000.

Alexandre G de Brevern, Hélène Valadié, Serge Hazout, and Catherine Etchebest. Extension of a local backbone description using a structural alphabet: a new approach to the sequence-structure relationship. *Protein Science*, 11(12):2871–2886, 2002.

Edo Dotan, Gal Jaschek, Tal Pupko, and Yonatan Belinkov. Effect of tokenization on transformers for biological sequences. *Bioinformatics*, 40(4):btae196, 2024.

Janani Durairaj, Mehmet Akdel, Dick de Ridder, and Aalt DJ van Dijk. Geometricus represents protein structures as shape-mers derived from moment invariants. *Bioinformatics*, 36(Supplement_2): i718–i725, 2020.

Sam Gelman, Bryce Johnson, Chase R Freschlin, Arnav Sharma, Sameer D'Costa, John Peters, Anthony Gitter, and Philip A Romero. Biophysics-based protein language models for protein engineering. *Nature Methods*, pp. 1–12, 2025.

Thomas Hayes, Roshan Rao, Halil Akin, Nicholas J Sofroniew, Deniz Oktay, Zeming Lin, Robert Verkuil, Vincent Q Tran, Jonathan Deaton, Marius Wiggert, et al. Simulating 500 million years of evolution with a language model. *Science*, 387(6736):850–858, 2025.

Michael Heinzinger, Konstantin Weissenow, Joaquin Gomez Sanchez, Adrian Henkel, Milot Mirdita, Martin Steinegger, and Burkhard Rost. Bilingual language model for protein sequence and structure. *NAR Genomics and Bioinformatics*, 6(4):lqae150, 2024.

Ioan Ieremie, Rob M Ewing, and Mahesan Niranjan. Protein language models meet reduced amino acid alphabets. *Bioinformatics*, 40(2):btae061, 2024.

Andriy Kryshtafovych, Torsten Schwede, Maya Topf, Krzysztof Fidelis, and John Moult. Critical assessment of methods of protein structure prediction (casp)—round xiv. *Proteins: Structure, Function, and Bioinformatics*, 89(12):1607–1617, 2021.

Tim Kucera, Carlos Oliver, Dexiong Chen, and Karsten Borgwardt. Proteinshake: Building datasets and benchmarks for deep learning on protein structures. *Advances in Neural Information Processing Systems*, 36:58277–58289, 2023.

N Jesper Larsson and Alistair Moffat. Off-line dictionary-based compression. *Proceedings of the IEEE*, 88(11):1722–1732, 2002.

Mingchen Li, Yang Tan, Xinzhu Ma, Bozitao Zhong, Huiqun Yu, Ziyi Zhou, Wanli Ouyang, Bingxin Zhou, Pan Tan, and Liang Hong. Prosst: Protein language modeling with quantized structure and disentangled attention. *Advances in Neural Information Processing Systems*, 37:35700–35726, 2024.

Xiaohan Lin, Zhenyu Chen, Yanheng Li, Zicheng Ma, Chuanliu Fan, Ziqiang Cao, Shihao Feng, Yi Qin Gao, and Jun Zhang. Tokenizing foldable protein structures with machine-learned artificial amino-acid vocabulary. *bioRxiv*, pp. 2023–11, 2023a.

Zeming Lin, Halil Akin, Roshan Rao, Brian Hie, Zhongkai Zhu, Wenting Lu, Nikita Smetanin, Robert Verkuil, Ori Kabeli, Yaniv Shmueli, et al. Evolutionary-scale prediction of atomic-level protein structure with a language model. *Science*, 379(6637):1123–1130, 2023b.

LeAnn M Lindsey, Nicole L Pershing, Anisa Habib, Keith Dufault-Thompson, W Zac Stephens, Anne J Blaschke, Xiaofang Jiang, and Hari Sundar. The impact of tokenizer selection in genomic language models. *Bioinformatics*, pp. btaf456, 2025.

Craig O Mackenzie. A tertiary alphabet for the observable protein structural universe captures sequence-structure relationships. *Protein Sci*, 25:75, 2016.

Swapnil Mahajan, Alexandre G de Brevern, Yves-Henri Sanejouand, Narayanaswamy Srinivasan, and Bernard Offmann. Use of a structural alphabet to find compatible folds for amino acid sequences. *Protein Science*, 24(1):145–153, 2015.

Eric Nguyen, Michael Poli, Marjan Faizi, Armin Thomas, Michael Wornow, Callum Birch-Sykes, Stefano Massaroli, Aman Patel, Clayton Rabideau, Yoshua Bengio, et al. Hyenadna: Long-range genomic sequence modeling at single nucleotide resolution. *Advances in neural information processing systems*, 36:43177–43201, 2023.

Gregory A Petsko and Dagmar Ringe. *Protein structure and function*. New Science Press, 2004.

Roshan Rao, Nicholas Bhattacharya, Neil Thomas, Yan Duan, Peter Chen, John Canny, Pieter Abbeel, and Yun Song. Evaluating protein transfer learning with tape. *Advances in neural information processing systems*, 32, 2019.

Alexander Rives, Joshua Meier, Tom Sercu, Siddharth Goyal, Zeming Lin, Jason Liu, Demi Guo, Myle Ott, C Lawrence Zitnick, Jerry Ma, et al. Biological structure and function emerge from scaling unsupervised learning to 250 million protein sequences. *Proceedings of the National Academy of Sciences*, 118(15):e2016239118, 2021.

Xavier Robin, Juergen Haas, Rafal Gumienny, Anna Smolinski, Gerardo Tauriello, and Torsten Schwede. Continuous automated model evaluation (cameo)—perspectives on the future of fully automated evaluation of structure prediction methods. *Proteins: Structure, Function, and Bioinformatics*, 89(12):1977–1986, 2021.

Jin Su, Chenchen Han, Yuyang Zhou, Junjie Shan, Xibin Zhou, and Fajie Yuan. Saprot: Protein language modeling with structure-aware vocabulary. *BioRxiv*, pp. 2023–10, 2023.

Burak Suyunu, Enes Taylan, and Arzucan Özgür. Linguistic laws meet protein sequences: A comparative analysis of subword tokenization methods. In *2024 IEEE International Conference on Bioinformatics and Biomedicine (BIBM)*, pp. 4489–4496. IEEE, 2024.

Yang Tan, Mingchen Li, Ziyi Zhou, Pan Tan, Huiqun Yu, Guisheng Fan, and Liang Hong. Peta: evaluating the impact of protein transfer learning with sub-word tokenization on downstream applications. *Journal of Cheminformatics*, 16(1):92, 2024.

Aaron Van Den Oord, Oriol Vinyals, et al. Neural discrete representation learning. *Advances in neural information processing systems*, 30, 2017.

Michel Van Kempen, Stephanie S Kim, Charlotte Tumescheit, Milot Mirdita, Jeongjae Lee, Cameron LM Gilchrist, Johannes Söding, and Martin Steinegger. Fast and accurate protein structure search with foldseek. *Nature biotechnology*, 42(2):243–246, 2024.

Yann Vander Meersche, Gabriel Cretin, Aria Gheeraert, Jean-Christophe Gelly, and Tatiana Galochkina. Atlas: protein flexibility description from atomistic molecular dynamics simulations. *Nucleic acids research*, 52(D1):D384–D392, 2024.

Iyanar Vetrivel, Swapnil Mahajan, Manoj Tyagi, Lionel Hoffmann, Yves-Henri Sanejouand, Narayanaswamy Srinivasan, Alexandre G De Brevern, Frédéric Cadet, and Bernard Offmann. Knowledge-based prediction of protein backbone conformation using a structural alphabet. *PloS one*, 12(11):e0186215, 2017.

Kevin K Yang, Niccolò Zanichelli, and Hugh Yeh. Masked inverse folding with sequence transfer for protein representation learning. *Protein Engineering, Design and Selection*, 36:gzad015, 2023.

Xinyu Yuan, Zichen Wang, Marcus Collins, and Huzefa Rangwala. Protein structure tokenization: Benchmarking and new recipe. *arXiv preprint arXiv:2503.00089*, 2025.

Baoquan Zhang, Huaibin Wang, Chuyao Luo, Xutao Li, Guotao Liang, Yunming Ye, Xiaochen Qi, and Yao He. Codebook transfer with part-of-speech for vector-quantized image modeling. In *Proceedings of the IEEE/CVF Conference on Computer Vision and Pattern Recognition*, pp. 7757–7766, 2024a.

Chengxin Zhang, Xi Zhang, Lydia Freddolino, and Yang Zhang. Biolip2: an updated structure database for biologically relevant ligand–protein interactions. *Nucleic Acids Research*, 52(D1): D404–D412, 2024b.

Jiayou Zhang, Barthelemy Meynard-Piganeau, James Gong, Xingyi Cheng, Yingtao Luo, Hugo Ly, Le Song, and Eric Xing. Balancing locality and reconstruction in protein structure tokenizer. *bioRxiv*, pp. 2024–12, 2024c.

Zhihan Zhou, Yanrong Ji, Weijian Li, Pratik Dutta, Ramana Davuluri, and Han Liu. Dnabert-2: Efficient foundation model and benchmark for multi-species genome. *arXiv preprint arXiv:2306.15006*, 2023.

A ABLATION STUDIES

Table 3: GEOBPE (1%) is trained with 1% of PDBs available during pretraining; GEOBPE (task-specific) directly uses PDBs in each downstream task. All use default value parameters in App. I.
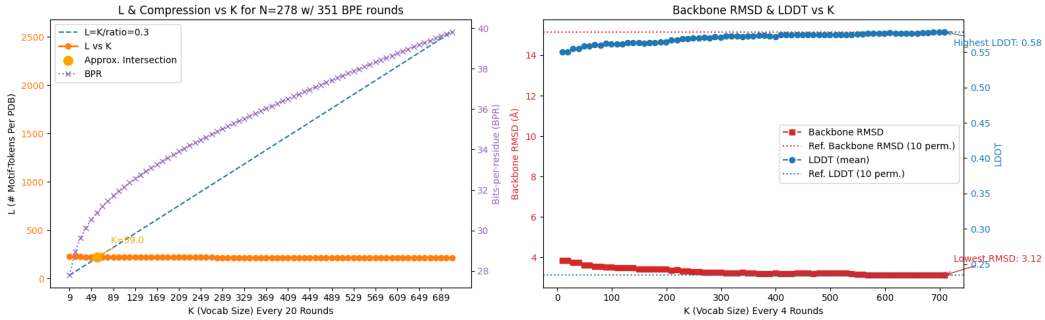
	Functional Site Prediction (AUROC%)															
Model	BindInt (Fold)	BindInt (SupFam)	BindBio (Fold)	BindBio (SupFam)	BindShake (Org)	CatInt (Fold)	CatInt (SupFam)	CatBio (Fold)	CatBio (SupFam)	Con (Fold)	Con (SupFam)	Rep (Fold)	Rep (SupFam)	Ept (Fold)	Ept (SupFam)	Avg
GEOBPE (1%)	59.98	90.17	95.00	95.89	87.73	66.28	88.87	94.95	95.95	71.75	84.56	56.37	72.87	63.83	77.55	80.12
GEOBPE	59.19	91.31	94.94	95.94	87.73	66.21	88.65	95.01	95.90	71.96	84.84	56.44	72.98	64.78	77.06	79.93
GEOBPE (task-specific)	60.16	89.93	95.05	95.92	87.73	66.28	88.82	94.98	95.90	71.85	85.92	56.33	72.72	64.78	77.04	80.23

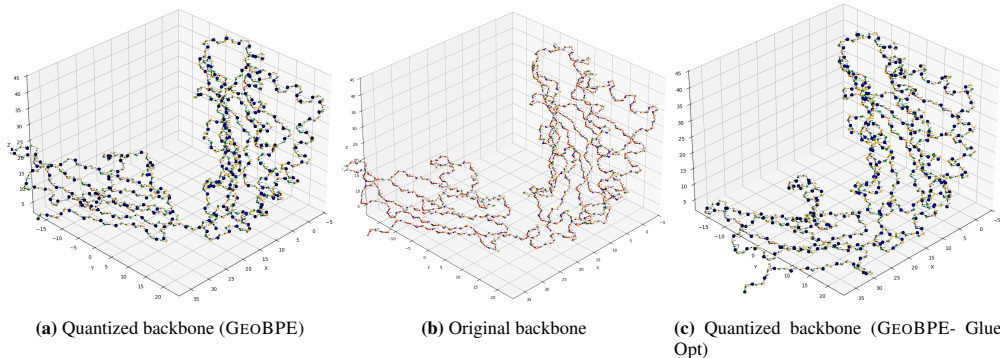|	Physicochemical Property Prediction (Spearman's ρ%)							Structure Property Prediction (Macro F1%)			
Model	FlexRMSF (Fold)	FlexRMSF (SupFam)	FlexBFactor (Fold)	FlexBFactor (SupFam)	FlexNEQ (Fold)	FlexNEQ (SupFam)	Avg	Homo (Fold)	Homo (SupFam)	Homo (Fam)	Avg
GEOBPE (1%)	40.42	47.55	34.74	32.21	56.78	55.32	44.50	21.65	50.25	84.87	52.26
GEOBPE	40.89	47.17	37.28	35.61	56.65	53.98	45.26	23.60	47.28	85.75	52.21
GEOBPE (task-specific)	39.39	44.00	37.94	38.36	56.22	54.22	45.02	24.22	46.58	84.57	51.79

GEOBPE is task-agnostic, and using task-specific data does not increase performance. For each task i, let $\mathsf{T}_i^{\text{task}}$ be a tokenizer fitted using only $\mathcal{D}_i^{\text{train}}$ (with its own vocabulary $\mathcal{V}_i$ but the same feature extractor F_Θ), and define $r_{\mathcal{V}_i}(\mathbf{x}) = \Psi_{\mathcal{V}_i}(F_\Theta(\mathbf{x}))$. We follow the same downstream transfer evaluation. We find an interesting result in Table 3, where directly training on the task-specific dataset does not meaningful change downstream prediction results. A closer look reveals the underlying reason is because the individual tokens do not differ significantly; motifs added to $\mathcal{V}$, in order, are similar across both GEOBPE and GEOBPE (task-specific). We can interpret this both positively and negatively. GEOBPE is insensitive to task-specific data and learns the "language" of protein folds consistently. This may be desirable for reusability of a tokenizer, as one does not need to retrain it for different data distributions, as all protein folds obey the same universal principles (Petsko & Ringe, 2004). At the same time, this upper bound tests whether the tokenizer can tailor its vocabulary to individual datasets for potentially higher scores, indicating GEOBPE by itself may lack the parameter capacity to overfit to individual tasks.

GEOBPE reaches comparable downstream transfer performance with 1% of data. In Table 3, we see GEOBPE fitted on just 1% of the pretraining data is enough to transfer, on average, the same amount of performance downstream as GEOBPE trained on the full dataset. There are no meaningful differences between GEOBPE and GEOBPE (1%), with GEOBPE doing 1.7% better on physicochemical property prediction and GEOBPE (1%) doing better 0.2% better on functionals ite prediction. These findings can be interpreted both positively and negatively for GEOBPE induced features: (1) they are *extremely* data-efficient, learning useful signals to transfer downstream with as few as 300 PDB structures; (2) they *underfit* the data, with no noticeable improvements for more data. Taken together, these findings imply GEOBPE is a lightweight add-on on top of any pretrained features Θ, but feeding more data to GEOBPE yields diminishing returns quickly.

Figure 4: We plot the BPR (purple), length (orange), backbone distortion (RMSD, LDDT) as $|\mathcal{V}|$ across BPE steps. Ref. backbone RMSD/LDDT (dotted lines) uses random angle values for all internal angles, sampled from the empirical angle distribution.

GEOBPE is multi-resolution, revealing finer details as more tokens are introduced. In Fig. 4, we run a coarse-grained version of GEOBPE (small initial $|\mathcal{V}|$) to observe an interesting feature of GEOBPE's design. As newly introduced tokens *re*-quantize the occurrences from the original data (span gathering step in Alg. 9, tokenization can adaptively *increase* the resolution if the new prototypes better capture the modes of variability for those occurrences than their previous quantization. We expose this via hyperparameters `bins` & `num_p` (see App. I), which tradeoff the super-resolution effect against coarse-graining effect at different token sizes, offering fine-grained control.

13

(a) Quantized backbone (GEOBPE)   (b) Original backbone   (c) Quantized backbone (GEOBPE- Glue Opt)

Figure 5: We ran an ablation for GEOBPE version with $|\mathcal{V}| = 600$, keeping all parameters the same but toggling whether glue opt is skipped in Alg. 16. We visualize the original (center), GEOBPE (left) and GEOBPE without glue opt (right) backbone states.

Rigid body refinment as an essential step for preserving fold integrity. If we omit the glue optimization from Algs 16 and 9 altogether, we see the effects in Fig. 5. For that experiment, we find avg. RMSD increase $1.66 \rightarrow 4.39$, and avg. LDDT drop $0.73 \rightarrow 0.69$ when glue opt is turned off. Rigid body refinement preserves the overall fold and modular architecture; turning it off causes individual domains to distort – the parallel strands drift apart – as well as the overall configuration to lose its integrity. Over the course of many time steps, global drift accumulate as local rounding occurs. Rigid body refinement is an indispensable subroutine for ensuring the overall quantization faithfully reproduces the fold integrity.

Increasing M_{max} beyond a certain threshold does not yield additional distortion benefits. We did a study comparing GEOBPE ($\mathcal{V} = 6000$, $M_{\mathrm{max}} \leftarrow 5000$, full settings in App. I) with "higher-resolution" settings `bins` $\leftarrow \{1 : 5000\}$, $M_{\mathrm{max}} \leftarrow 20000$. Interestingly, we found overall RMSD/LDDT did *not* improve (1.40 vs 1.39, 0.76 vs 0.75, both in favor of the incumbent) despite increased computational expenditure spent on Alg. 8. The most likely explanation is there is no marginal utility increasing M_{max} beyond 5000, and differences in distortion rates are likely due to the numerical stability of Alg. 10 more so than the hyperparameters.

B   DATASET DETAILS

Training. For training GEOBPE, we started with the pretraining data splits released by Yuan et al. (2025), which follows the same criteria used to train the OpenFold2 model Ahdritz et al. (2024). For VanillaVQ and AminoASeed baselines, we use the same splits as Yuan et al. (2025) directly. For GEOBPE, we further filtered the data down to only ones with complete backbone information (e.g. backbone dihedrals are not NaN, each residue contains N, CA and C), resulting in 34818 structures. We further excluded structures shorter than 40 or longer than 512 residues, resulting in 33992 structures for training GeoBPE and 3810 for validation (only used for E).

Held-out testing. We use CAMEO and CASP14 test sets for evaluating the generalization of tokenizers (Robin et al., 2021; Kryshtafovych et al., 2021). For CASP14, we follow Yuan et al. (2025) and select only proteins released after the pretraining data cutoff date.

Downstream Tasks. Our 8 downstream tasks cover a breadth of structure and function-related predictions. They are divided into 3 categories and are assembled from 6 sources: InterPro (BindInt, Con, Rep) (Blum et al., 2025), BioLIP2 (BindBio, CatBio) (Zhang et al., 2024b), ProteinShake (BindShake) (Kucera et al., 2023), ProteinGLUE (Ept) (Capel et al., 2022), TAPE (Homo) (Rao et al., 2019) and ATLAS (FlexRMSF, FlexBFactor, FlexNEQ) (Vander Meersche et al., 2024).

1. **Functional site prediction**: Binding site prediction (BindInt), catalytic site (CatInt), conserved site prediction (Con), repeat motif prediction (Rep), epitope region prediction (Ept)
2. **Physicochemical property prediction**: Structural flexibility prediction, measured using metric RMSF (FlexRMSF), B-factor (FlexBFactor) and Neq (FlexNEQ)
3. **Structure classification** (protein-level): Remote homology detection (Homo)

Functional site prediction tasks predict whether each residue is in a site of functional importance (binding, catalytic activity or antibody recognition) or part of an evolutionary motif (conserved site or part of a repeated motif). PSTs which learn semantically meaningful signals like motif boundaries are expected to perform well on these tasks.

Physicochemical property prediction tasks predict the flexibility of each residue as a continuous value. Higher flexibility can be a clue that the residue may be more amenable to functional activity. PSTs that capture a fine-grained view of the localized protein dynamics are expected to predict residue-level flexibility well.

Remote homology detection is a multi-class fold classification problem. Proteins which belong to the same fold class can be distantly related or share similar functions on the whole. Therefore, PSTs that capture the overall fold-level geometry are expected to do well on this task.

For more dataset statistics and preparation details, see Yuan et al. (2025).

C ADDITIONAL RESULTS

Table 4 contains additional tasks Rep, Ept, FlexRMSF, and FlexBFactor. Table 5 contains additional task data Repeat, Ept, Atlas, Homo. Task abbrevations were defined in App. B.

Table 4: Additional downstream transfer performance tasks. Setup follows Table 1.

Task	Split	Continuous PST		Discrete PST					
		ProteinMPNN	MIF	FoldSeek	ProTokens	ESM3	VanillaVQ	AminoAseed	GEOBPE (v.s. ESM3)
Functional Site Prediction (AUROC%)									
Rep	Fold	77.63	74.53	47.71	53.20	74.70	**75.99**	74.97	56.44 (-24.44%)
	SupFam	80.71	83.11	52.54	77.25	82.36	82.09	**84.57**	72.98 (-11.39%)
Ept	Fold	62.84	68.78	54.56	52.49	63.69	59.28	62.16	**64.78 +1.71%**
	SupFam	64.84	82.98	50.53	61.92	61.97	67.24	72.02	**77.06 +24.35%**
Physicochemical Property Prediction (Spearman's ρ%)									
FlexBFactor	Fold	31.88	34.60	4.17	6.67	23.60	22.32	21.30	**37.28 (+57.97%)**
	SupFam	34.56	35.23	6.99	5.47	25.80	23.73	21.76	**35.61 (+38.02%)**
FlexNEQ	Fold	69.69	65.32	5.71	12.98	45.05	35.95	49.64	**56.65 (+25.75%)**
	SupFam	68.69	64.82	2.66	10.51	35.45	35.61	50.15	**53.98 (+52.27%)**

Table 5: Additional expert agreement results. Setup follows Table 2.

		Rep	Ept	Atlas	Homo
Domain	Mean Recall	99.93 (99.34)	100 (100.0)	99.93 (90.47)	99.98 (100.0)
	Mean Precision	99.2 (43.59)	99.75 (77.89)	98.44 (31.29)	99 (41.92)
	Mean F1	99.56 (81.86)	99.87 (82.68)	99.17 (67.37)	99.48 (79.07)
	Mean IOU	99.12 (82.18)	99.75 (82.68)	98.37 (67.07)	98.98 (78.78)
Segment	Mean Recall	100 (100.0)	100 (100.0)	100 (100.0)	100 (100.0)
	Mean Precision	98.76 (61.93)	95.52 (60.8)	96.09 (47.29)	95.91 (54.13)
	Mean F1	99.38 (61.93)	97.68 (60.8)	98 (47.29)	97.91 (54.13)

D TOKEN EFFICIENCY METRICS

Let $v = \{1, \ldots, K\}$ denote the codebook (size K). Given a corpus tokenized into a flat list of code indices, let c_j be the count of code j and $N = \sum_{j=1}^{K} c_j$ the total token count. We define the empirical unigram distribution

$$p(j) = \frac{c_j}{N} \quad \text{for } j \in v.$$

Utilization rate (UR). UR measures how many distinct codes are actually used:

$$\text{UR} = \frac{1}{K} \left| \{ j \in v : c_j > 0 \} \right| \in [0, 1].$$

We report UR in percent. UR is important for diagnosing codebook collapse, a well-known phenomenon in VQ-VAEs where only a small number of codes are actively used Zhang et al. (2024a). This creates a quantization bottleneck, handicapping the tokenizer's performance and efficiency Yuan et al. (2025).

Unigram entropy and perplexity. Using the Shannon entropy (natural logarithm),

$$H = -\sum_{j \in v} p(j) \log p(j), \qquad \mathrm{PPL} = \exp(H).$$

This *codebook perplexity* reflects how uniformly codes are used (model-free, ignores sequence context).

Max-normalized perplexity. Because the maximum entropy at uniform is $\log K$ (hence $\mathrm{PPL}_{\max} = K$), we also report the scale-free ratio

$$\widetilde{\mathrm{PPL}} = \frac{\mathrm{PPL}}{K} = \exp\left(\frac{H}{\log K} \cdot \log K\right) \frac{1}{K} = \exp\left(H - \log K\right) \in (0, 1].$$

Table 6: We evaluate token efficiency of GEOBPE across varying $|\mathcal{V}| \in \{600, 2500, 6000\}$, as reported in Figure 3.

Method	Codebook Size	UR (%)		Perplexity	
		CAMEO	CASP14	CAMEO	CASP14
VQ-VAE	512	5.55	5.60	0.034	0.0337
AminoASeed	512	64.45	68.87	0.495	0.5119
ESM3	4096	27.60	32.10	0.249	0.2841
FoldSeek	20	99.00	100.00	0.755	0.7435
ProToken	512	69.88	75.56	0.537	0.5697
PT-BPE	600	59.81	39.48	0.397	0.403
	2500	58.24	38.22	0.274	0.264
	6000	53.73	31.30	0.242	0.222

Table 7: We adopt the Small Structure Language Model evaluation protocol described in App. E. We sample 100 PDB structures.

			Small Structure Language Model Evaluation		
Method	Codebook Size	scTM	Designability (scTM \textgreater 0.5)	1-Diversity (mean TM)	Uniqueness (TM=0.5)
VQ-VAE	512	0.205	1%	0.752	98%
AminoASeed	512	0.186	1%	0.476	16%
PT-BPE	600	0.268	3%	0.768	99%
	2500	0.267	3%	0.766	99%
	6000	0.277	4%	0.763	98%

E SMALL STRUCTURE LANGUAGE MODEL EVALUATION

This section specifies the protocol used to evaluate generative efficiency via training a small decoder-only LM over the joint geometric vocabulary learned by GEOBPE. It incorporates the mask constraints used at generation time (Alg. 4) during training to ensure consistency between training and sampling. The same procedure is used for evaluating VQ-VAEs. For training and sampling, the only difference is dropping the mask constraints. For inference, the samples are passed through the VQ-VAE decoder to construct backbone coordinates instead of assembling the backbone directly via Alg. 5. This required considerably more resources, and we discuss how we implemented this in App. E.6.

E.1 DATA PREPARATION AND SPLITS

Tokenization. We construct the joint vocabulary Σ (Alg. 14) and convert each protein t_τ into a token sequence $x^{(\tau)} = (x_1^{(\tau)}, \ldots, x_{L_\tau}^{(\tau)})$ via BACKBONETOSEQUENCE (Alg. 15). Sequences alternate

---

Algorithm 2 GEOLM-PRETRAIN — decoder-only next-token prediction on geometric tokens

---

Require: Corpus of proteins $\{t_\tau\}_{\tau=1}^T$ with final segmentations $\{\mathcal{P}^{(\tau)}\}$ and assigned medoids; joint vocabulary Σ and tokenizers from Alg. 14, 15; a decoder-only Transformer $\mathsf{Tr}_\theta : \Sigma^* \to \Delta^{|\Sigma|}$ with causal mask; special BOS/EOS (optional); training steps S, optimizer $\mathcal{O}$.
Ensure: Trained parameters θ.

1: **Dataset construction.** For each τ, build $x^{(\tau)} = \text{BACKBONETOSEQUENCE}(t_\tau)$ (Alg. 15). Let $L_\tau = |x^{(\tau)}|$.
2: **Objective.** For any sequence $x = (x_1, \ldots, x_L)$, define

$$\mathcal{L}_{\text{NTP}}(\theta;\, x) = -\sum_{t=1}^{L-1} \log p_\theta\big(x_{t+1} \mid x_{\leq t}\big), \quad p_\theta(\cdot | x_{\leq t}) = \text{softmax}\big(\mathsf{Tr}_\theta(x_{\leq t})\big).$$

3: **Training loop.**
4: **for** $s = 1$ **to** S **do**
5:　　Sample a minibatch $\mathcal{B} \subset \{1, \ldots, T\}$.
6:　　$\mathcal{L} \leftarrow \dfrac{1}{|\mathcal{B}|} \displaystyle\sum_{\tau \in \mathcal{B}} \mathcal{L}_{\text{NTP}}(\theta;\, x^{(\tau)})$.
7:　　Update $\theta \leftarrow \mathcal{O}\big(\theta,\, \nabla_\theta \mathcal{L}\big)$.
8: **end for**
9: **return** θ.

Algorithm 3 BUILDEMPIRICALPRIORS — length prior and first-token prior

---

Require: Training corpus of tokenized backbones $\{x^{(\tau)} = (x_1^{(\tau)}, \ldots, x_{L_\tau}^{(\tau)})\}_{\tau=1}^T$ constructed by Alg. 15 (motif, then θ, ω, ϕ, repeating); valid sequence lengths satisfy $L_\tau \equiv 1 \pmod 4$ and end in a *terminating* motif token.
Ensure: Discrete priors Π_L on lengths K and Π_{start} on the first token.

1: **Length prior:** for every K with $K \equiv 1 \pmod 4$, set

$$\Pi_L(K) \propto \Big|\big\{\tau :\ L_\tau = K\big\}\Big| \text{ and normalize } \sum_K \Pi_L(K) = 1.$$

2: **First-token prior:** over motif tokens only, set

$$\Pi_{\text{start}}(i) \propto \Big|\big\{\tau :\ x_1^{(\tau)} = i\big\}\Big|, \quad i \in \Sigma_{\text{med}}; \quad \sum_{i \in \Sigma_{\text{med}}} \Pi_{\text{start}}(i) = 1.$$

3: **return** $\Pi_L,\ \Pi_{\text{start}}$.

---

strictly motif $\to \theta \to \omega \to \phi \to$ motif $\to \cdots$ and end with a *terminating* motif token (length-2 bond–residue class), hence $L_\tau \equiv 1 \pmod 4$.

Splits. We partition proteins at the *protein level* into train/validation/test (e.g., 80/10/10) to prevent leakage across chains.

E.2 TRAINING OBJECTIVE WITH STRUCTURAL MASKS

We train a causal Transformer Tr_θ with teacher forcing. To enforce legality at each position t, we apply the same *type mask by position modulo 4* used in generation (Alg. 4):

$$t \equiv 1 \pmod 4 \Rightarrow \Sigma_{\text{med}}, \quad t \equiv 2 \Rightarrow \Sigma_\theta, \quad t \equiv 3 \Rightarrow \Sigma_\omega, \quad t \equiv 0 \Rightarrow \Sigma_\phi,$$

setting logits for all other token types to $-\infty$ before the softmax.

Termination constraint at motif slots. At motif positions ($t \equiv 1 \pmod 4$), we impose the same termination rule as in Alg. 4: (i) if $t < L_\tau$, mask out terminating motifs Σ_{term}; (ii) if $t = L_\tau$, mask out non-terminating motifs.

Loss. With masks applied, the negative log-likelihood is

$$\mathcal{L}_{\text{NTP}}(\theta; x^{(\tau)}) = -\sum_{t=1}^{L_\tau - 1} \log p_\theta\Big(x_{t+1}^{(\tau)} \mid x_{\leq t}^{(\tau)}\Big), \qquad p_\theta(\cdot \mid x_{\leq t}) = \text{softmax}(\tilde{z}_t),$$

Algorithm 4 UNCONDITIONALGEOLMGENERATE — motif/glue token generation

---

Require: Trained decoder-only Transformer Tr_θ with vocabulary Σ from Alg. 14; id blocks

$$\Sigma_{\mathrm{med}} = \{1, \ldots, M\} \tag{1}$$
$$\Sigma_\theta = \{M+1, \ldots, M+B_\theta\} \tag{2}$$
$$\Sigma_\omega = \{M+B_\theta+1, \ldots, M+B_\theta+B_\omega\} \tag{3}$$
$$\Sigma_\phi = \{M+B_\theta+B_\omega+1, \ldots, M+B_\theta+B_\omega+B_\phi\}; \tag{4}$$

terminating-motif set $\Sigma_{\mathrm{term}} \subseteq \Sigma_{\mathrm{med}}$ (motifs in the length-2 bond-residue class); priors $\Pi_L, \Pi_{\mathrm{start}}$ (Alg. 3); temperature $\tau > 0$; maximum length $K_{\max}$; number of samples S.

Ensure: S unconstrained token sequences $\{x^{(s)}\}$ alternating motif and glue tokens and ending in a terminating motif.

1: Define the **type mask by position** (t starts at 1):

$$t \equiv 1 \ (\mathrm{mod}\ 4) \Rightarrow \mathrm{motif}\ (\Sigma_{\mathrm{med}}), \quad t \equiv 2 \Rightarrow \theta\ (\Sigma_\theta), \quad t \equiv 3 \Rightarrow \omega\ (\Sigma_\omega), \quad t \equiv 0 \Rightarrow \phi\ (\Sigma_\phi).$$

2: **for** $s = 1$ **to** S **do**
3:      Sample a target cap $K^{\mathrm{cap}} \sim \Pi_L$ and set $K^{\mathrm{cap}} \leftarrow \min(K^{\mathrm{cap}}, K_{\max})$.
4:      Sample the first token $x_1^{(s)} \sim \Pi_{\mathrm{start}}$ (so $x_1^{(s)} \in \Sigma_{\mathrm{med}}$).
5:      **for** $t = 2, 3, \ldots, K^{\mathrm{cap}}$ **do**
6:          Compute last-position logits $z_t = \mathsf{Tr}_\theta\big(x_{1:t-1}^{(s)}\big)$ with causal masking; let $v = |\Sigma|$.
7:          Build a **hard mask** $m \in \mathbb{R}^v$ initialized to $-\infty$ and set:

$$\begin{cases} m_i \leftarrow 0 & \text{if } t \equiv 1\ (4) \text{ and } i \in \Sigma_{\mathrm{med}}, \\ m_i \leftarrow 0 & \text{if } t \equiv 2\ (4) \text{ and } i \in \Sigma_\theta, \\ m_i \leftarrow 0 & \text{if } t \equiv 3\ (4) \text{ and } i \in \Sigma_\omega, \\ m_i \leftarrow 0 & \text{if } t \equiv 0\ (4) \text{ and } i \in \Sigma_\phi. \end{cases}$$

8:          **Termination constraint at motif positions:**
       •   If $t \equiv 1\ (4)$ and $t < K^{\mathrm{cap}}$, then *disallow* early stop: set $m_i \leftarrow -\infty$ for all $i \in \Sigma_{\mathrm{term}}$.
       •   If $t \equiv 1\ (4)$ and $t = K^{\mathrm{cap}}$, then *force* stop: set $m_i \leftarrow -\infty$ for all $i \in \Sigma_{\mathrm{med}} \setminus \Sigma_{\mathrm{term}}$.
9:          Form masked logits $\tilde{z}_t = z_t + m$ and sample

$$x_t^{(s)} \sim \mathrm{Categorical}(\mathrm{softmax}(\tilde{z}_t/\tau)).$$

10:          **(Optional early stop)** If $t \equiv 1\ (4)$ and $x_t^{(s)} \in \Sigma_{\mathrm{term}}$, then **break**.
11:      **end for**
12: **end for**
13: **return** $\{x^{(s)}\}_{s=1}^S$.

---

where $\tilde{z}_t$ are masked logits. We optimize θ by minimizing the average NLL over the training set.

Early stopping. We select checkpoints by validation loss with a patience of 5 epochs.

E.3   UNCONDITIONAL SAMPLING FOR QUALITATIVE EVALUATION

Empirical priors. We form the *length prior* Π_L and *first-token prior* Π_{start} from the training corpus using BUILDEMPIRICALPRIORS (Alg. 3). Π_L is supported on legal lengths $K \equiv 1 \ (\mathrm{mod}\ 4)$; Π_{start} is over Σ_{med}.

Constrained generation. We sample with UNCONDITIONALGEOLMGENERATE (Alg. 4): draw $K^{\mathrm{cap}} \sim \Pi_L$ (clipped by a maximum), sample the first motif $x_1 \sim \Pi_{\mathrm{start}}$, then autoregress under the same positional type mask and termination constraint as training. Temperature and nucleus sampling are optional ablations.

GEOBPE Dequantization and assembly. Generated token sequences are mapped to full backbones via DEQUANTIZEANDASSEMBLE (Alg. 5): medoid tokens decode to internal coordinates over their motif spans; glue-bin tokens decode to bin-midpoint angles; forward kinematics with the seeded entry frame yields atom coordinates $\{(N_i, \mathrm{CA}_i, C_i)\}_{i=1}^{\widehat{N}}$.

Algorithm 5 DEQUANTIZEANDASSEMBLE — from tokens to a full backbone

---

Require: One generated sequence $x = (x_1, \ldots, x_L)$ from Alg. 4; medoid dictionary $\{\mathrm{id}_{\mathrm{med}}(\kappa, j) \mapsto \Pi_j^{(\kappa)}\}$ where each prototype $\Pi_j^{(\kappa)}$ is a tuple of internal coordinates for a motif $\mathcal{M}$; glue bin edges $\{\beta_b^\theta\}_{b=0}^{B_\theta}, \{\beta_b^\omega\}_{b=0}^{B_\omega}, \{\beta_b^\phi\}_{b=0}^{B_\phi}$ (circular edges for angles, linear for lengths if used); canonical seed triad $(N_\star, \mathrm{CA}_\star, C_\star)$ and SEEDTRIAD.

Ensure: A complete backbone $\{(N_i, \mathrm{CA}_i, C_i) \in \mathbb{R}^3\}_{i=1}^{\widehat{N}}$ assembled from the decoded motifs and glues.

1: **Parse tokens into motifs and glues (fixed 4-cycle).** Let the motif indices be $t \in \{1, 5, 9, \ldots\}$; write $x_t = \mathrm{id}_{\mathrm{med}}(\kappa^{(m)}, j^{(m)})$ for $m = 1, \ldots, M$ where $M = \frac{L+3}{4}$. For each boundary $m = 1, \ldots, M-1$, decode the three bins:

$$b_\theta = x_{4m-2} - M, \quad b_\omega = x_{4m-1} - (M + B_\theta), \quad b_\phi = x_{4m} - (M + B_\theta + B_\omega),$$

and **dequantize** to the bin midpoints

$$\bar{\theta}_m = \tfrac{1}{2}(\beta_{b_\theta - 1}^\theta + \beta_{b_\theta}^\theta), \quad \bar{\omega}_m = \tfrac{1}{2}(\beta_{b_\omega - 1}^\omega + \beta_{b_\omega}^\omega), \quad \bar{\phi}_m = \tfrac{1}{2}(\beta_{b_\phi - 1}^\phi + \beta_{b_\phi}^\phi).$$

2: **Recover internal coordinates.** For each motif m, let $\Pi_{j^{(m)}}^{(\kappa^{(m)})}$ provide the internal bond lengths ℓ, bond angles θ, and dihedrals (ψ, ω, ϕ) *across its span* $\mathcal{M}^{(m)}$. Construct its internal entry→exit transform $T_{(m)}^{\mathrm{int}}$ (product of link transforms G_i inside the motif; see Preliminaries).

3: **Forward kinematics assembly.**

4: Initialize the entry frame by seeding the very first residue: $(N_1, \mathrm{CA}_1, C_1) \leftarrow \mathrm{SEEDTRIAD}(1)$ and form $F_1 = (R_1, t_1)$ as in the Entry/Exit frame definition.

5: **Motif 1:** Traverse the links inside $\mathcal{M}^{(1)}$ using its internal coordinates to compute frames $F_2, \ldots, F_{q_1}$ (and atom positions) by repeated G_i multiplications; set the current exit frame $F_{(1)}^{\mathrm{exit}} = F_{q_1}$.

6: **for** $m = 1$ **to** $M - 1$ **do**

7:     **Boundary glue:** form the boundary transform

$$T_{(m)}^{\mathrm{glue}} = G_{q_m}(\theta^{CNCA} = \bar{\theta}_m, \ \omega = \bar{\omega}_m, \ \phi = \bar{\phi}_m),$$

    i.e., the SE(3) map from the exit frame of $\mathcal{M}^{(m)}$ to the entry frame of $\mathcal{M}^{(m+1)}$ determined by the three dequantized glue angles (and adjacent bond lengths).

8:     Set the entry frame of $\mathcal{M}^{(m+1)}$ to

$$F_{(m+1)}^{\mathrm{entry}} \leftarrow T_{(m)}^{\mathrm{glue}} \ F_{(m)}^{\mathrm{exit}}.$$

9:     **Motif** $(m+1)$**:** traverse its internal links to produce all residue frames and atom positions; update $F_{(m+1)}^{\mathrm{exit}}$.

10: **end for**

11: **Concatenate atoms.** Collect the atoms from all traversals in order, yielding the backbone $\{(N_i, \mathrm{CA}_i, C_i)\}_{i=1}^{\widehat{N}}$, where $\widehat{N}$ is the total number of residues implied by the concatenated motif spans (the final motif is guaranteed terminating).

12: **return** the complete backbone coordinates.

E.4 GENERATIVE QUALITY ASSESSMENT

We evaluate unconditional samples produced by UNCONDITIONALGEOLMGENERATE (Alg. 4) and assembled by DEQUANTIZEANDASSEMBLE (Alg. 5) using four structure-centric metrics based on TM-score.[1]

Setup. From each model we draw a fixed number of backbones $\{\widehat{\mathcal{B}}_n\}_{n=1}^N$ (legal lengths, terminal motif constraint). Unless noted, metrics are computed on these *backbone geometries* without further post-processing.

(1) scTM (self-consistency TM-score). For each generated backbone $\widehat{\mathcal{B}}$, we (i) design a sequence $\widehat{s}$ with a standard inverse-folding model, (ii) predict a structure $\widetilde{\mathcal{B}}$ from $\widehat{s}$ using a single-structure predictor (e.g., ESMFold), and (iii) compute

$$\mathrm{scTM}(\widehat{\mathcal{B}}) = \mathrm{TM\text{-}score}(\widetilde{\mathcal{B}}, \widehat{\mathcal{B}}).$$

We report the mean scTM over the N samples.

---

[1]TM-score is obtained with a standard implementation (e.g., TM-align); higher is better.

(2) Designability (% with scTM > 0.5). A backbone is deemed *designable* if its self-consistency exceeds the canonical threshold 0.5:

$$\text{Designability} = \frac{1}{N} \sum_{n=1}^{N} \mathbf{1}\Big\{ \text{scTM}(\widehat{\mathcal{B}}_n) > 0.5 \Big\} \times 100\%.$$

This is the fraction of samples for which a designed sequence refolds back to the generated backbone at the fold level.

(3) Diversity (mean pairwise TM). To quantify sample-to-sample diversity, we compute the mean pairwise TM-score across the set (lower is more diverse):

$$\text{Diversity} = \frac{2}{N(N-1)} \sum_{1 \le i < j \le N} \text{TM-score}\big(\widehat{\mathcal{B}}_i, \, \widehat{\mathcal{B}}_j\big).$$

(When N is large, we estimate this by uniform sub-sampling of pairs.)

(4) Uniqueness (% non-duplicates at TM < 0.5). We mark a sample as *unique* if its nearest neighbor among the other generated backbones has TM-score < 0.5:

$$\text{Uniqueness} = \frac{1}{N} \sum_{n=1}^{N} \mathbf{1}\Big\{ \max_{m \ne n} \text{TM-score}\big(\widehat{\mathcal{B}}_n, \widehat{\mathcal{B}}_m\big) < 0.5 \Big\} \times 100\%.$$

This measures the proportion of samples that are not near-duplicates under a fold-level threshold.

Reporting. For each model we report the four metrics above on the same set size N (and the same sampling priors and temperature). Codebook size and token perplexity are *not* used in these downstream comparisons.

E.5 GENERATED BACKBONES

(a) Generated backbone with scTM score 0.50 **(b)** Generated backbone with scTM score 0.56

Figure 6: We visualize two backbones generated by GEOBPE with default settings reported in App. I during SSLM-Eval.

In Fig. 6a, we see a long, well-structured and assembled α-helix, which is one of the most common and stable secondary structures in proteins. The curved helical cap at the top resembles a common N-terminal capping motif, which often stabilizes helices through hydrogen bonding networks or electrostatic interactions. Such elongated α-helices are commonly found in transmembrane helices or coiled-coil domains which are involved in dimerization and DNA-binding. The overall curvature and spatial continuity also suggest potential compatibility with membrane proteins or structural scaffolds, especially behave as substance binding receptors as well as ion channels.

In Fig. 6b, we see a structure that resembles DNA-binding motifs or cytokine folds, which are quite well-known for cellular signaling or regulation. The geometric density of this structure also suggests a pre-organized hydrophobic core, which is critical for proper folding and stability in the cytoplasmic environment. This structure exhibits a compact bundle of helices with apparent crossing angles which are similar to some small globular domains in common protein structures. The folding appears non-linear but in a quite controlled, manner which suggests potential tertiary structure forming interactions such as hydrophobic-hydrophobic interaction.

E.6 IMPLEMENTATION DETAILS

SSLM-Eval GEOBPE implementation and hardware details. We train a small autoregressive Transformer on discretized geometry tokens. We use a hidden size $d_{\text{model}} = 256$, $L = 8$ Transformer layers with GELU activations, $H = 8$ attention heads, and feed-forward width $d_{\text{ff}} = 1024$. Token and positional embeddings are summed, a LayerNorm is applied before the classifier, and the output projection is weight–tied to the token embedding. A causal attention mask enforces left-to-right prediction. Sequences are padded to a dataset-dependent maximum length (the 95th percentile of training lengths by default). We optimize cross-entropy loss with Adam (learning rate 1×10^{-4}), batch size 32, for up to 100 epochs with early stopping on validation perplexity. For unconditional generation, we sample 100 sequences at temperature 1.0, drawing target lengths from the empirical length prior (restricted to valid lengths by construction) and the first token from the empirical start-token prior; decoding proceeds token-by-token under the causal mask. On a single GPU, one epoch takes just under 10 mins and converges in ≈ 60 epochs (can vary across tokenizer settings). The data splits are the same as those for pretraining (see App. B) – $33992, 3810$ training/validation structures for GEOBPE.

SSLM-Eval VQ-VAE implementation and hardware details. We extend the distributed Lightning setup of Yuan et al. (2025) with a self-contained evaluation step at the end of each validation epoch. Using 4 ranks, each GPU accumulates the epoch's quantized token sequences from training and validation; these are gathered and passed to a lightweight auxiliary trainer that uses the same SSLM-Eval (GEOBPE) script and hyperparameters. After convergence, we sample 100 new token sequences, decode them with the VQ-VAE decoder into backbone coordinates, and write PDBs to a directory named by the current epoch. We compute all non-SCTM metrics locally, then distribute a heavier SCTM evaluation across ranks on sharded PDB subsets. Each rank produces its shard's results, and rank-0 merges them into a single summary that is logged to the trainer.

F EXPERT AGREEMENT METRICS

Our method segments a protein sequence into M contiguous residue spans $P_j = [p_j, q_j]$ with $q_j + 1 = p_{j+1}$ for $j = 1, \ldots, M - 1$. We compare these segments against N ground-truth domain annotations $D_i = [s_i, e_i]$. All sets below are sets of integer residue indices and $|\cdot|$ denotes cardinality (length in residues). We report (i) *domain-level* alignment quality for each true domain using the best consecutive block of predicted segments, and (ii) *segment-level* detection statistics at an Intersection-over-Union (IoU) threshold τ. This combination captures both *how well* each domain is covered and *how economically* the predicted segments explain the annotations, while remaining robust to small boundary jitter.

Annotation source. Ground-truth domains come from **CATH FunFams** Das et al. (2015b). They are functional families defined by *profile HMM* hits trained on primary-sequence data Das et al. (2015a;b). Our evaluation thus measures how well the predicted segmentation aligns with functionally coherent families derived from sequence-based HMM models.

In our setting, individual predicted segments tend to be substantially shorter than the curated domain annotations. A naive one-to-one comparison would systematically penalize predictions that must be *combined* to cover a domain. To ensure a fair comparison, for each D_i we first select the single best *consecutive* block of predicted segments S_i that maximizes IoU with D_i (below), then compute per-domain scores and *macro-average* them so that each domain contributes equally, independent of its length.

Notation and best block per domain. For domains $D_i = [s_i, e_i]$ ($i = 1{:}N$) and predicted segments $P_j = [p_j, q_j]$ ($j = 1{:}M$, with $q_j{+}1 = p_{j+1}$), define

$$(a_i, b_i) \in \arg \max_{1 \le m \le n \le M} \frac{\left| D_i \cap \bigcup_{k=m}^{n} P_k \right|}{\left| D_i \cup \bigcup_{k=m}^{n} P_k \right|}, \qquad S_i := \bigcup_{k=a_i}^{b_i} P_k.$$

(Ties may prefer the shortest S_i or fewest segments.)

Domain-level scores (macro). Let $\text{ov}_i = |D_i \cap S_i|$, $|D_i| = e_i - s_i + 1$, $|S_i| = \sum_{k=a_i}^{b_i} (q_k - p_k + 1)$. Then

$$\text{Recall}_i = \frac{\text{ov}_i}{|D_i|}, \quad \text{Precision}_i = \frac{\text{ov}_i}{|S_i|}, \quad F_{1,i} = \frac{2 \, \text{Recall}_i \, \text{Precision}_i}{\text{Recall}_i + \text{Precision}_i}, \quad \text{IoU}_i = \frac{\text{ov}_i}{|D_i| + |S_i| - \text{ov}_i}.$$

Macro-averages:

$$\overline{\mathrm{Recall}} = \tfrac{1}{N}\sum_i \mathrm{Recall}_i, \quad \overline{\mathrm{Precision}} = \tfrac{1}{N}\sum_i \mathrm{Precision}_i, \quad \overline{F_1} = \tfrac{1}{N}\sum_i F_{1,i}, \quad \overline{\mathrm{IoU}} = \tfrac{1}{N}\sum_i \mathrm{IoU}_i.$$

Interpretation: recall rewards coverage; precision rewards compactness of S_i; F_1 balances both; IoU is thresholdable and scale-invariant.

Segment-level detection at IoU threshold τ. Let $\mathcal{U} = \bigcup_{i:\,\mathrm{IoU}_i \geq \tau}\{a_i, \ldots, b_i\}$. Define

$$\mathrm{SegPrec} = \frac{|\mathcal{U}|}{M}, \qquad \mathrm{SegRec} = \frac{|\{\,i : \mathrm{IoU}_i \geq \tau\,\}|}{N}, \qquad \mathrm{SegF}_1 = \frac{2\,\mathrm{SegPrec}\,\mathrm{SegRec}}{\mathrm{SegPrec} + \mathrm{SegRec}}.$$

Interpretation: SegPrec penalizes unused segments; SegRec penalizes missed/poorly aligned domains. Sweeping τ yields a PR curve.

Randomization baseline and reporting. Using 1000 uniform random partitions into M contiguous spans of the same sequence, recompute all metrics under the same best-block protocol and average over runs. We report using the format:

$$\text{ours (random-avg)},$$

e.g., $\overline{\mathrm{IoU}} = 0.47\,(0.18)$.

Notes. In degenerate cases (e.g., $|S_i| = 0$ or a zero denominator), we adopt the standard convention of returning 0 for the affected ratio or F_1 term.

Together, the domain-level (overlap-quality) metrics and the segment-level (parsimony and coverage) metrics directly test the two desiderata of protein-domain segmentation: (i) accurate coverage of each domain with minimal spillover, and (ii) a parsimonious set of segments that explain as many domains as possible. Macro-averaging after selecting the best block per domain ensures fairness when predicted segments are shorter than annotated domains, and the permutation baseline quantifies how far performance rises above chance given the same M.
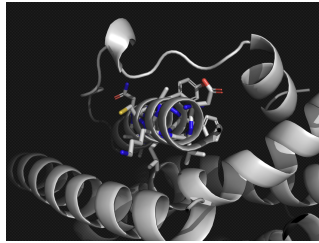
G EXPERT CASE STUDIES

Individual Tokens Correspond to Secondary Structures. Figure 7 is an example of a single token GEOBPE discovers. It features an alpha helix that includes aromatic cage (formed by Tryptophan / Tyrosine) and hydrogen bonding residue. It can be a common structure in Nucleotide-recognition domains, especially the hydrogen bond donors/acceptors can serve for specific molecular recognition (e.g., methylated lysines, nucleotide bases or acetyl groups) as well as Neurotransmitter receptors. From interpretation, this motif is functionally specific.

It can serve as ligand binding pocket, which is tightly packed and evolutionarily conserved. This could behave significantly in substance recognition. The tightly packed helical scaffold in this separated motif is likely stabilizing the motif's geometry and ensuring specificity. Motif-scaffold synergy can also help to define a structure's rigidity and flexibility.
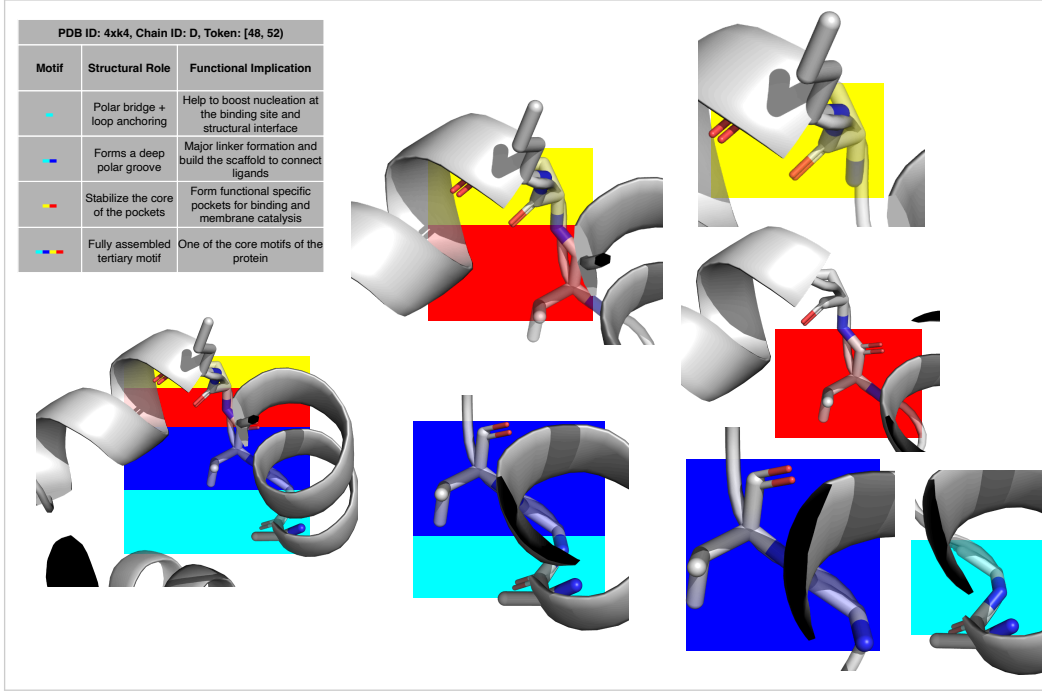
Merge Hierarchy of GEOBPE Reflects Combination of Secondary Structures for Driving Function.

Figure 8. 4xk4 is the human mitochondrial carrier protein SLC25A20 (carnitine/acylcarnitine translocase). It's a transmembrane transport protein within the mitochondrial inner membrane, responsible for shuttling carnitine and acylcarnitine molecules across the membrane. This a process critical to fatty acid oxidation and energy metabolism. The core motif that the algorithm separated out contain three similar domains, each with two transmembrane helices and a loop. It appears to lie deep within the transmembrane domain, forming part of the central binding cavity. From this know-how information, the 48-4 motif is really significant in the following three aspects:

Figure 7: An exemplary GEOBPE token spans backbone atoms of an alpha helix (colored).

1. It will serve for substrate recognition where the internal polar residues bind to the acylcarnitine or carnitine head group via ionic and hydrogen bonds. It will also alter the transition state of the

Figure 8: Chain D of PDB 4xk4. Hierarchical Merge Tree for Token [48, 52]. GEOBPE arrived at this token by merging [48, 49) with [49, 50), [50, 51) with [51, 52), and [48, 50) with [50, 52).

during the transport cycles. For example, this motif can play a role in shift conformation between open-to-cytoplasm and open-to-matrix states.
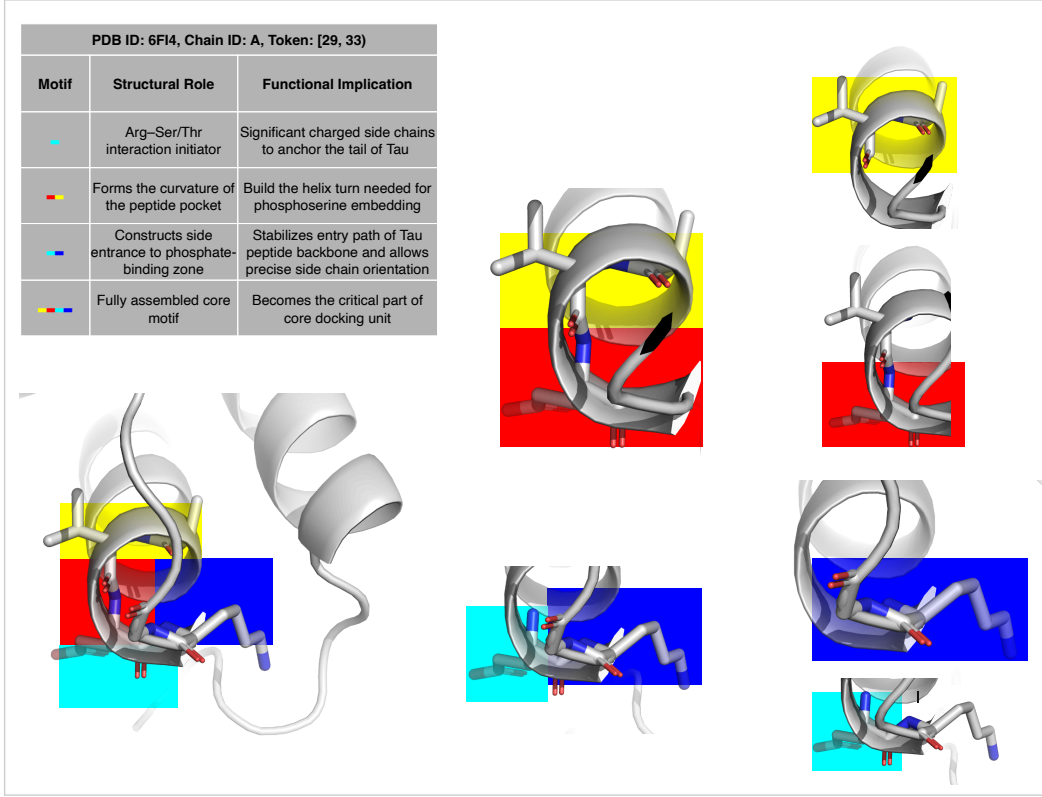
2. We also observe similar motifs are found in other SLC25 family members (e.g., ADP/ATP carriers), indicating a shared mechanism of transport.

3. While the broader transmembrane region is dominated by repetitive helices, this localized motif exhibits a unique composition of diverse side chains, polar residues, and tightly packed interactions, reinforcing its functional specificity.

Figure 9. 6FI4 is the crystal structure of a hybrid peptide composed of a C-terminally modified Tau protein segment bound to the human 14-3-3σ protein, solved at 2.0 Å resolution via X-ray crystallography. 14-3-3 proteins are a family of conserved regulatory molecules that bind phosphoserine/phosphothreonine-containing motifs on target proteins and are central to cell cycle control, apoptosis, transcriptional regulation, and signal transduction. The hybrid peptide mimics Tau phosphorylation, which is relevant to neurodegenerative disease pathology like Alzheimer's disease. From this know-how information, the 29-4 motif is significant in the following two aspects:

1. Phosphopeptide recognition and improve the binding Stability: This motif orchestrates recognition of the Tau-derived phosphoserine motif via a precise network of hydrogen bonds and electrostatic complementarity. The Lys/Arg residues (seen in blue) form salt bridges with phosphate groups, stabilizing the interaction.

2. The structure shared recognition fold across the 14-3-3 protein family: This motif, with its basic side chain tunnel and surrounding helices, represents a canonical recognition site. Similar structural motifs are observed in all 14-3-3 isozymes when binding phosphoproteins and will serve for post-translational modification signaling.

H   COMPUTATIONAL COMPLEXITY

Notation. Let $\{t^{(\tau)}\}_{\tau=1}^{T}$ be T backbones with lengths $N^{(\tau)}$, and let $N := \sum_{\tau=1}^{T} N^{(\tau)}$ be the total residues. In each STEP iteration, the most frequent geo-pair key has M_t occurrences. We use K for the number of medoids produced when clustering a key's occurrences (a small constant in practice). For k-medoids we either: (i) cluster all M_t items, or (ii) cap with $M_{\max}$ items. Let P be the *period*

Figure 9: Chain A of PDB 6FI4. Hierarchical Merge Tree for Token [29, 33). GEOBPE arrived at this token by merging [29, 30) with [30, 31), [31, 32) with [32, 33), and [29, 31) with [31, 33).

at which GLUEOPTALL is invoked (see Alg. 9), and let C_{IK} denote the cost of one global IK pass (see below). The ordered map $\mathcal{D}$ stores key $\rightarrow$ occurrence-set with a priority $(\rho, -|\mathcal{O}|, \kappa)$; each insert/erase in $\mathcal{D}$ costs $O(\log |\mathcal{D}|) = O(\log N)$.

Component building blocks.

- **k-medoids on m items:** $O(m^2)$ to build the pairwise RMSD matrix (constant fragment length), plus a small constant number of assignment/update steps
- **Priority map updates:** each merge touches $O(1)$ neighbor pairs; across the *entire* run there are $O(N)$ merges $\Rightarrow O(N \log N)$ total map operations Every merge eliminates one boundary and touches at most its two neighbors, so the total number of insert/erase operations in $\mathcal{D}$ across the full run is $O(N)$; with $O(\log N)$ per op, the total is $O(N \log N)$.
- **Global IK (GLUEOPTALL) one pass:** forward kinematics is linear in links, so one pass costs $C_{\text{IK}} = O(N \cdot S_{\text{FK}})$, where S_{FK} is the (small) number of optimizer steps $\times$ the constant forward/backward cost per link Periodic GLUEOPTALL adds $\frac{T}{P} O(N \log N)$ due to re-keying affected boundaries.

Worst-case complexity (no subsampling cap).

- **ResInitTokens:** $O(N^2) + O(N \log N)$.
- **Step loop over all iterations:** $O\left(\sum_t M_t^2\right) + O(N \log N)$.
- **Periodic global glue opt:** $\frac{T}{P}\left(C_{\text{IK}} + O(N \log N)\right)$.
- **Total (worst case):** $O(N^2) + O\left(\sum_t M_t^2\right) + O(N \log N) + \frac{T}{P}\left(C_{\text{IK}} + O(N \log N)\right)$.
- **Total (with cap):** $O(M_{\max}^2) + O(T M_{\max}^2) + O(N \log N) + \frac{T}{P}\left(C_{\text{IK}} + O(N \log N)\right)$.

24

In the worst case $M_t = \Theta(N)$ for many steps, $\sum_t M_t^2$ can reach $\Theta(N^2)$. Here $M_{\max}$ controls runtime. Putting it together, we can make the following statements about GEOBPE's computational complexity:

- **Training (discovering the vocabulary):** dominated by k-medoids calls and periodic IK:

$$O\big(T\,M_{\max}^2\big) + O(N \log N) + \tfrac{T}{P}\big(C_{\text{IK}} + O(N \log N)\big).$$

- **Tokenization (apply a learned vocabulary):** similar to training but without any k-medoids calls and in terms of $N^{(\tau)}$:

$$O(N^{(\tau)} \log N^{(\tau)}) + \tfrac{T}{P}\big(C_{\text{IK}} + O(N^{(\tau)} \log N^{(\tau)})\big).$$

- **Detokenization (geometry reconstruction):** forward kinematics per link is $O(1)$; reconstructing all atoms is $O(N)$.

Insights for efficient practice. (i) Most structural variability concentrates in a small number of modes; a modest $M_{\max}$ suffices. (ii) Dictionary updates are *incremental*; our implementation uses an ordered map. (iii) In practice, we choose $P = 10$; GlueOptAll calls are infrequent enough it does not become an issue. If this becomes the practical bottleneck, we recommend GLUEOPT for local IK updates instead, which drops the $O(N \log N)$ term.

Distortion is insensitive to $M_{\max}$. In App. A, we observe that increasing $M_{\max}$ yields no real gains beyond 5000; any marginal gains are lost to the subsequent GlueOptAll call. This is because medoids stabilize quickly on representative modes, capping clustering with $M_{\max}$ preserves reconstruction quality while bounding the dominant $O(M_{\max}^2)$ term. This is backed by observations made by de Brevern et al. (2002); Mackenzie (2016) and others that the structural universe of possible elements are captured by a exponentially smaller number of modes.

I HYPERPARAMETER SETTINGS

We describe the key parameters that govern GEOBPE's behaviors in Table 8. For each, we report the default setting used by GeoBPE across most key results of the paper: Fig. 3, Tables 6 & 7 and App. A. We report any instances overriding the default settings here:

1. Token efficiency / SSLM-Eval (Tables 6, 7) set `num_p` $\leftarrow$ $\{2:500, 3:2000\}$, `bins` $\leftarrow$ $\{1:1000\}$ for codebook size $|\mathcal{V}| = 2500$ and `num_p` $\leftarrow$ $\{2:1000, 3:5000\}$, `bins` $\leftarrow$ $\{1:2000\}$ for $|\mathcal{V}| = 6000$.
2. Pareto-efficiency evaluation (Fig 3) further add the setting for $|\mathcal{V}| = 21000$ where `num_p` $\leftarrow$ $\{2:1000, 3:20000\}$, `bins` $\leftarrow$ $\{1:2000\}$. Varying `num_p` elastically moves along the Pareto-efficiency plot, trading off BPR for distortion.
3. Downstream transfer experiments (Tables 1, 5) set `num_p` $\leftarrow$ $\{2:2, 3:5, 5:1, 6:2, 8:1\}$ and `bins` $\leftarrow$ $\{1 : 50\}$, and `bin_strategy` $\leftarrow$ histogram-cover to adaptively coarsen the resolution. GEOBPE prioritizes learning fine-to-coarse hierarchical signals over low distortion for effective transfer.

Table 8: We report the main hyperparameters that affect GEOBPE behavior.

Parameter	Value	Meaning	Default Behavior
`bin_strategy`	histogram	Controls the strategy for empirical quantizer estimation (Alg. 1)	numpy.histogram with `bins`
`bins`	$\{1:500\}$	Controls the number of bins used by `bin_strategy`	Uses 500 quantiles
`free_bonds`	True	Whether to quantize bond lengths	Don't standardize
		Setting to False standardizes all bond lengths to precomputed values	Quantize with linear histograms
`glue_opt`	True	Whether to do Glue Opt in Algs 16, 9	Do Glue Opt
`glue_opt_every`	10	How often to run global glue opt (final line of Alg. 9)	Do every 10 iters
`glue_opt_method`	all	Whether to do batch glue opt (Alg. 10) or single-boundary glue opt (Alg. 17)	Do batch glue opt
`glue_opt_prior`	1.0	Prior weight encouraging optimized glues to match empirical distribution	1.0
`max_num_strucs`	5000	Max number of occurrences for clustering ($M_{\max}$ in Alg. 6)	5000
`num_p`	$\{2:100, 3:500,$ $5:20, 6:100\}$	K determined by span length L in Alg. 6, L not in `num_p` round down to nearest key	Use $K = 100$ when $L = 2$ Use $K = 500$ when $L \geq 3$
`rmsd_super_res`	True	Whether to use occurrences from *original* backbone t_τ or current backbone in Alg. 9	Use original states

J LARGE LANGUAGE MODEL USAGE

We used LLMs mainly for polishing the writing, including prompts to check for grammar mistakes, improving clarity of mathematical notation, and formatting the text to save space.

K ALGORITHMIC DETAILS

Algorithm 6 RMSD_PARTITION on motif–pair occurrences

Require: Motif–pair occurrences $\mathcal{S} = \{u = 1, \ldots, M\}$ with $\mathcal{M}_{i_u:k_u}^{(t_u)}$, common span length $L = k_u - i_u + 1$, and either $\forall u, \ k_u = N^{(t_u)}$ or $\forall u, \ k_u < N^{(t_u)}$; target $K \geq 1$; optional $M_{\max}, T, \varepsilon$.

Ensure: Medoids $\widehat{\mathcal{M}} = \{\widehat{m}_1, \ldots, \widehat{m}_K\} \subseteq \mathcal{S}$ and assignments $c : \{1, \ldots, M\} \to \{1, \ldots, K\}$.

1: For each $u \in \mathcal{S}$, compute $\mathbf{X}_u \in \mathbb{R}^{3L \times 3}$ via COMPUTE_COORDS$(i_u:k_u)$.
2: Let $\mathcal{A} \subseteq \mathcal{S}$ be a uniform sample without replacement of size $\min(M, M_{\max})$ (or $\mathcal{A} = \mathcal{S}$).
3: Build $D \in \mathbb{R}^{|\mathcal{A}| \times |\mathcal{A}|}$ with $D_{uv} = $ KABSCH_RMSD$(\mathbf{X}_u, \mathbf{X}_v)$ for $u, v \in \mathcal{A}$.
4: Initialize $\mathcal{M} \leftarrow \{m_1, \ldots, m_K\}$ as K distinct uniform indices from $\{1, \ldots, |\mathcal{A}|\}$.
5: **for** $t = 1$ **to** T **do**
6:    Assign: $c(u) \leftarrow \arg\min_{j \in \{1,\ldots,K\}} D_{u,m_j}$ for all $u \in \mathcal{A}$.
7:    Update each j: $\mathcal{C}_j = \{u \in \mathcal{A} : c(u) = j\}$. If $\mathcal{C}_j = \emptyset$, reseed m_j uniformly from $\mathcal{A}$; else

$$m'_j \leftarrow \arg\min_{u \in \mathcal{C}_j} \sum_{v \in \mathcal{C}_j} D_{uv}.$$

8:    If $\sum_{j=1}^K D_{m_j, m'_j} < \varepsilon$ **break**; else set $m_j \leftarrow m'_j$ for all j.
9: **end for**
10: Map $\mathcal{M} = \{m_1, \ldots, m_K\}$ (indices in $\mathcal{A}$) to $\widehat{\mathcal{M}} = \{\widehat{m}_1, \ldots, \widehat{m}_K\}$ (indices in $\mathcal{S}$).
11: For each $u \in \mathcal{S}$, set $c(u) \leftarrow \arg\min_{j \in \{1,\ldots,K\}}$ KABSCH_RMSD$(\mathbf{X}_u, \mathbf{X}_{\widehat{m}_j})$.
12: **return** $\widehat{\mathcal{M}}$ and $c(\cdot)$.

Algorithm 7 KABSCH_RMSD$(\mathbf{P}, \mathbf{Q})$

Require: $\mathbf{P}, \mathbf{Q} \in \mathbb{R}^{n \times 3}$ with $n = 3L$.
1: $\bar{\mathbf{p}} = \frac{1}{n} \sum_i \mathbf{P}_i, \ \bar{\mathbf{q}} = \frac{1}{n} \sum_i \mathbf{Q}_i$
2: $\tilde{\mathbf{P}} = \mathbf{P} - \bar{\mathbf{p}}, \quad \tilde{\mathbf{Q}} = \mathbf{Q} - \bar{\mathbf{q}}$
3: $\mathbf{H} = \tilde{\mathbf{P}}^\top \tilde{\mathbf{Q}}, \quad \mathbf{U} \Sigma \mathbf{V}^\top = \text{SVD}(\mathbf{H})$
4: $\mathbf{R} = \mathbf{U}\mathbf{V}^\top$; if $\det(\mathbf{R}) < 0$, set $\mathbf{V}_{:,3} \leftarrow -\mathbf{V}_{:,3}$ and recompute $\mathbf{R} = \mathbf{U}\mathbf{V}^\top$
5: $\mathbf{Q}_{\text{aligned}} = (\mathbf{Q} - \bar{\mathbf{q}})\mathbf{R}^\top + \bar{\mathbf{p}}$
6: **return** $\sqrt{\frac{1}{n} \sum_{i=1}^n \|\mathbf{P}_i - \mathbf{Q}_{\text{aligned},i}\|^2}$

Algorithm 8 K_MEDOIDS on a precomputed distance matrix

Require: Symmetric $D \in \mathbb{R}^{N \times N}$, number of clusters K, iterations T, tolerance ε.

Ensure: Medoid set $\{m_1, \ldots, m_K\}$ and assignments $c(\cdot)$ on $\{1, \ldots, N\}$.
1: Initialize medoids $\{m_j\}$ as K distinct random indices.
2: **for** $t = 1$ **to** T **do**
3:    $c(u) \leftarrow \arg\min_j D_{u,m_j}$ for all u
4:    **for** $j = 1$ **to** K **do**
5:        $\mathcal{C}_j = \{u : c(u) = j\}$; if $\mathcal{C}_j = \emptyset$, re-seed m_j at random
6:        $m'_j \leftarrow \arg\min_{u \in \mathcal{C}_j} \sum_{v \in \mathcal{C}_j} D_{uv}$
7:    **end for**
8:    If $\sum_{j=1}^K D_{m_j, m'_j} < \varepsilon$, **break**; else $m_j \leftarrow m'_j$ for all j
9: **end for**
10: **return** $\{m_j\}$ and $c(\cdot)$

Algorithm 9 STEP — one GEOBPE merge iteration

Require: Current segmentations $\{\mathcal{P}^{(\tau)}\}_{\tau=1}^{T}$ and merge hierarchies $\{\mathcal{F}^{(\tau)}\}_{\tau=1}^{T}$ (frontier leaves of $\mathcal{F}^{(\tau)}$ equal $\mathcal{P}^{(\tau)}$); priority-ordered map $\mathcal{D}$ with keys $\pi(\kappa) = (\rho(\kappa), -|\mathcal{O}(\kappa)|, \kappa)$ and values $\mathcal{O}(\kappa)$; current vocabulary $\mathcal{V}$ (map: key → prototype set); boundary-glue quantizers $Q_{\theta^{CNCA}}, Q_{\omega}, Q_{\phi}$; optional glue mode ∈ {*none, each, all*} and, if *all*, a period.
Ensure: Updated $(\{\mathcal{P}^{(\tau)}\}, \{\mathcal{F}^{(\tau)}\}, \mathcal{D}, \mathcal{V})$.
 1: **Select the merge key.**
$$\big((\rho^{\star}, -c^{\star}, \kappa^{\star}), \mathcal{O}(\kappa^{\star})\big) \leftarrow \text{FRONT}(\mathcal{D}).$$

   Write each occurrence as $(\mathcal{L}, \mathcal{R}) \in \mathcal{O}(\kappa^{\star})$ with $\mathcal{L} = \mathcal{M}_{p:q}^{(t_\tau)}$ and $\mathcal{R} = \mathcal{M}_{q+1:r}^{(t_\tau)}$.
 2: **Prototype assignment (create-or-assign).**
 3: **if** $\rho^{\star} = 1$ (*no prototypes yet*) **then**
 4:   Gather concatenated spans $\{\mathcal{M}_{p:r}^{(t_\tau)}\}$ from *original* t_τ for all $(\mathcal{L}, \mathcal{R}) \in \mathcal{O}(\kappa^{\star})$ (identical length).
 5:   Run RMSD_PARTITION (Alg. 6) to obtain medoids and $c : \mathcal{O}(\kappa^{\star}) \rightarrow \{1, \ldots, K_{\kappa^{\star}}\}$.
 6:   Define $\mathcal{A}_{\kappa^{\star}} = \{\Pi_j^{(\kappa^{\star})}\}_{j=1}^{K_{\kappa^{\star}}}$ (medoid spans' internal-parameter tuples).
 7:   Update vocabulary: $\mathcal{V}[\kappa^{\star}] \leftarrow \mathcal{A}_{\kappa^{\star}}$ and set $\rho^{\star} \leftarrow 0$.
 8: **else**
 9:   For each occurrence, set $c(\mathcal{L}, \mathcal{R}) = \arg\min_j \text{RMSD}\big(\mathcal{M}_{p:r}^{(t_\tau)}, \Pi_j^{(\kappa^{\star})}\big)$ using $\mathcal{V}[\kappa^{\star}]$.
10: **end if**
11: **Greedy, non-overlapping merges (and hierarchy updates).** For each backbone t_τ, sort occurrences by p and choose a maximal disjoint subset $S^{(\tau)}$ left-to-right. For every $(\mathcal{L}, \mathcal{R}) \in S^{(\tau)}$ with label $j = c(\mathcal{L}, \mathcal{R})$:
   1. **Form merged motif** $\widetilde{\mathcal{M}} = \mathcal{M}_{p:r}^{(t_\tau)}$ and *overwrite* its internals by the prototype:
   $$\big(\ell, \theta, \psi, \omega, \phi, \{\Gamma_i\}\big)\big|_{\widetilde{\mathcal{M}}} \leftarrow \Pi_j^{(\kappa^{\star})}.$$

   2. **Update segmentation** $\mathcal{P}^{(\tau)}$: replace $(\mathcal{L}, \mathcal{R})$ by $\widetilde{\mathcal{M}}$.
   3. **Update hierarchy** $\mathcal{F}^{(\tau)}$: add a *parent* node for span $[p{:}r]$ with left child the node of $\mathcal{L}$ and right child the node of $\mathcal{R}$; update the *frontier* (replace the two leaves by their parent so the frontier again equals $\mathcal{P}^{(\tau)}$).
   4. **(Optional) single-boundary glue opt** at link $p{-}1 \rightarrow p$ if mode=*each*; re-snap the three boundary angles.
12: **Update counts and priorities in** $\mathcal{D}$. For each merged $(\mathcal{L}, \mathcal{R})$:
   1. **Merged pair decrement:** remove this occurrence from $\mathcal{O}(\kappa^{\star})$; let the new count be c_{new}. Erase $\pi_{\text{old}} = (0, -c^{\star}, \kappa^{\star})$ and, if $c_{\text{new}} > 0$, insert $(0, -c_{\text{new}}, \kappa^{\star}) \mapsto \mathcal{O}(\kappa^{\star})$.
   2. **Neighbor decrements:** with neighbors $\mathcal{L}^{-}$ and $\mathcal{R}^{+}$ (when defined), compute $k_L = \text{COMPUTEGEOKEY}(\mathcal{L}^{-}, \mathcal{L})$ and $k_R = \text{COMPUTEGEOKEY}(\mathcal{R}, \mathcal{R}^{+})$. For each $k \in \{k_L, k_R\}$ whose count decreases to c_{new}, erase $(\rho(k), -c_{\text{old}}, k)$ and, if $c_{\text{new}} > 0$, insert $(\rho(k), -c_{\text{new}}, k)$.
   3. **Neighbor increments:** compute $k'_L = \text{COMPUTEGEOKEY}(\mathcal{L}^{-}, \widetilde{\mathcal{M}})$ and $k'_R = \text{COMPUTEGEOKEY}(\widetilde{\mathcal{M}}, \mathcal{R}^{+})$ (when defined); increment their counts and (re)insert with priorities $(\rho(k), -c_{\text{new}}, k)$, where $\rho(k) = \mathbf{1}[k \notin \text{dom}(\mathcal{V})]$.
13: **(Optional periodic global glue opt).** If mode=*all* and the schedule triggers, apply GLUEOPTALL (Alg. 10) to all modified backbones; recompute keys for their adjacent pairs, and for every affected key k, perform the same erase/insert priority update with $\rho(k) = \mathbf{1}[k \notin \text{dom}(\mathcal{V})]$. If FRONT($\mathcal{D}$) then exposes a recurring key ($\rho = 0$) promoted by glue refinement, immediately re-invoke STEP (no new clustering).
14: **return** $\{\mathcal{P}^{(\tau)}\}, \{\mathcal{F}^{(\tau)}\}, \mathcal{D},$ and $\mathcal{V}$.

Algorithm 10 GLUEOPTALL — global differentiable inverse kinematics over glue angles

---

Require: Medoids $\widehat{\mathcal{M}}$ and assignments $c(\cdot)$ from RMSD_PARTITION; occurrences $\mathcal{S} = \{u\}$ with spans $\mathcal{M}_{i_u:k_u}^{(t_u)}$; target frames $F_i^{\star,(t)} = (R_i^{\star,(t)}, t_i^{\star,(t)})$ (with $F_1^{\star,(t)}$ from SEEDTRIAD); weights (w_R, w_t); optimizer steps T and step size η

Ensure: Updated glues $\{\Gamma_i^{(t)}\}$ and frames $\{\widehat{F}_i^{(t)}\}$

1: **Snap internals:** for $u \in \mathcal{S}$, set internals of $\mathcal{M}_{i_u:k_u}^{(t_u)} \leftarrow$ those of its medoid $m(u) = \widehat{m}_{c(u)}$
2: **Init glues:** copy original $\Gamma_i^{(t)}$ for all backbones t and links $i = 1{:}N^{(t)}-1$ (these are the optimization variables)
3: **Loss:**

$$\mathcal{L}(\Gamma) = \sum_t \sum_{i=2}^{N^{(t)}} \Big(w_R \big\| \log((\widehat{R}_i^{(t)})^\top R_i^{\star,(t)}) \big\|_2^2 + w_t \big\| \widehat{t}_i^{(t)} - t_i^{\star,(t)} \big\|_2^2 \Big)$$

4: **Forward kinematics (FK):** with $\widehat{F}_1^{(t)} = F_1^{\star,(t)}$,

$$\widehat{F}_{i+1}^{(t)} = \widehat{F}_i^{(t)} \widehat{G}_i^{(t)} \big(\Gamma_i^{(t)}; \text{ current internals} \big), \quad \widehat{G}_i^{(t)} \text{ from internals and } \Gamma_i^{(t)} = \{\theta_i^{CNCA}, \psi_i, \phi_{i+1}\}^2$$

5: **Optimize glues (autodiff):** for $s = 1{:}T$:
6:    run FK, evaluate $\mathcal{L}$; backprop $\nabla_\Gamma \mathcal{L}$; update all $\Gamma_i^{(t)}$
7:    wrap $\psi, \phi \in (-\pi, \pi]$; project $\theta^{CNCA} \in (0, \pi)$
8: **return** $\{\Gamma_i^{(t)}\}, \{\widehat{F}_i^{(t)}\}$

Algorithm 11 BINARY TREE–LSTM CELL (Tai et al., 2015)

Require: Left $(h_\ell, c_\ell) \in \mathbb{R}^d \times \mathbb{R}^d$, right (h_r, c_r); $W \in \mathbb{R}^{5d \times 2d}, b \in \mathbb{R}^{5d}$
Ensure: $(h_p, c_p) \in \mathbb{R}^d \times \mathbb{R}^d$

1: $u \leftarrow \begin{bmatrix} h_\ell \\ h_r \end{bmatrix}; \quad \begin{bmatrix} i \\ f_\ell \\ f_r \\ o \\ g \end{bmatrix} \leftarrow W u + b$

2: $i, f_\ell, f_r, o \leftarrow \sigma(\cdot); \quad g \leftarrow \tanh(g)$
3: $c_p \leftarrow f_\ell \odot c_\ell + f_r \odot c_r + i \odot g$
4: $h_p \leftarrow o \odot \tanh(c_p)$
5: **return** (h_p, c_p)

Algorithm 12 DOWNWARD BINARY TREE–LSTM CELL

Require: Parent downward $(\bar{h}_p, \bar{c}_p) \in \mathbb{R}^d \times \mathbb{R}^d$, sibling upward (h_s, c_s); $\widetilde{W} \in \mathbb{R}^{5d \times 2d}, \widetilde{b} \in \mathbb{R}^{5d}$
Ensure: $(\bar{h}_c, \bar{c}_c) \in \mathbb{R}^d \times \mathbb{R}^d$

1: $u \leftarrow \begin{bmatrix} \bar{h}_p \\ h_s \end{bmatrix}; \quad \begin{bmatrix} \bar{i} \\ \bar{f}_p \\ \bar{f}_s \\ \bar{o} \\ \bar{g} \end{bmatrix} \leftarrow \widetilde{W} u + \widetilde{b}$

2: $\bar{i}, \bar{f}_p, \bar{f}_s, \bar{o} \leftarrow \sigma(\cdot); \quad \bar{g} \leftarrow \tanh(\bar{g})$
3: $\bar{c}_c \leftarrow \bar{f}_p \odot \bar{c}_p + \bar{f}_s \odot c_s + \bar{i} \odot \bar{g}$
4: $\bar{h}_c \leftarrow \bar{o} \odot \tanh(\bar{c}_c)$
5: **return** $(\bar{h}_c, \bar{c}_c)$

Algorithm 13 UP–DOWN TREE ENCODER ON A FOREST (one protein)

Require: Protein t_τ with $N^{(\tau)}$ residues; binary forest $\mathcal{F}^{(\tau)} = (V^{(\tau)}, E^{(\tau)})$ whose frontier (in order) is $\mathcal{P}^{(\tau)}$; leaf embeddings $\{e_i^{(\tau)} \in \mathbb{R}^d\}_{i=1}^{N^{(\tau)}}$ (e.g., ESM3[3]; internal-edge topological order $E^{(\tau)} = \{(p, \ell, r)\}$; roots $R^{(\tau)} \subset V^{(\tau)}$; parameters $\Theta = \{W, b, \widetilde{W}, \widetilde{b}\}$; combiner $\oplus \in \{\text{concat}, \text{sum}\}$.

Ensure: $z_\tau^{\text{prot}} \in \mathbb{R}^{d_z}$; $\{z_{\tau,i}^{\text{res}}\}_{i=1}^{N^{(\tau)}}$.

1: **Upward.** For leaves $i \le N^{(\tau)}$: $h_i^\uparrow \leftarrow e_i^{(\tau)}$, $c_i^\uparrow \leftarrow 0$. For $(p, \ell, r) \in E^{(\tau)}$ in order:

$$(h_p^\uparrow, c_p^\uparrow) \leftarrow \text{TREELSTMCELL}(h_\ell^\uparrow, c_\ell^\uparrow, \; h_r^\uparrow, c_r^\uparrow; \; W, b) \text{ (Alg. 11)}.$$

2: **Super-root.** $h_{\text{SR}}^\uparrow \leftarrow |R^{(\tau)}|^{-1} \sum_{r \in R^{(\tau)}} h_r^\uparrow$; set node SR with $(h_{\text{SR}}^\uparrow, c_{\text{SR}}^\uparrow = 0)$.

3: **Downward.** $(\bar{h}_{\text{SR}}, \bar{c}_{\text{SR}}) \leftarrow (0, 0)$. For each tree rooted at $r \in R^{(\tau)}$, recurse: for internal p with children (ℓ, r) and given $(\bar{h}_p, \bar{c}_p)$,

$$(\bar{h}_\ell, \bar{c}_\ell) \leftarrow \text{DOWNTREELSTM}((\bar{h}_p, \bar{c}_p), \; (h_r^\uparrow, c_r^\uparrow); \; \widetilde{W}, \widetilde{b}),$$

$$(\bar{h}_r, \bar{c}_r) \leftarrow \text{DOWNTREELSTM}((\bar{h}_p, \bar{c}_p), \; (h_\ell^\uparrow, c_\ell^\uparrow); \; \widetilde{W}, \widetilde{b}) \text{ (Alg. 12)}.$$

4: **Representations.** For any node v: $u_v^\downarrow \leftarrow \bar{h}_v$.

5: **if** $\oplus = $ concat **then**

6:     $z_{\tau,i}^{\text{res}} \leftarrow [h_i^\uparrow; u_i^\downarrow] \in \mathbb{R}^{2d}$ $(i{=}1{:}N^{(\tau)})$; $z_\tau^{\text{prot}} \leftarrow [h_{\text{SR}}^\uparrow; u_{\text{SR}}^\downarrow] \in \mathbb{R}^{2d}$

7: **else**

8:     $z_{\tau,i}^{\text{res}} \leftarrow h_i^\uparrow + u_i^\downarrow \in \mathbb{R}^d$ $(i{=}1{:}N^{(\tau)})$; $z_\tau^{\text{prot}} \leftarrow h_{\text{SR}}^\uparrow + u_{\text{SR}}^\downarrow \in \mathbb{R}^d$

9: **end if**

10: **return** $z_\tau^{\text{prot}}, \{z_{\tau,i}^{\text{res}}\}_{i=1}^{N^{(\tau)}}$.

Algorithm 14 BUILDJOINTVOCAB — medoids then glue–angle bins

Require: GEOBPE vocab $\mathcal{V} = \{\kappa \mapsto \mathcal{A}_\kappa\}$ with key introduction order $(\kappa^{(1)}, \ldots, \kappa^{(S)})$; medoids $\mathcal{A}_\kappa = \{\Pi_j^{(\kappa)}\}_{j=1}^{K_\kappa}$; glue quantizers $Q_{\theta^{CNCA}}, Q_\omega, Q_\phi$ with bin centers $\{\mu_b^\theta\}_{b=1}^{B_\theta}$, $\{\mu_b^\omega\}_{b=1}^{B_\omega}$, $\{\mu_b^\phi\}_{b=1}^{B_\phi}$

Ensure: Dictionary Σ; maps $\text{id}_{\text{med}} : (\kappa, j) \mapsto \{1, \ldots, |\Sigma_{\text{med}}|\}$ and $\text{id}_{\text{bin}} : (\text{type} \in \{\theta, \omega, \phi\}, b) \mapsto \{|\Sigma_{\text{med}}| + 1, \ldots, |\Sigma|\}$

1: **Medoids (in introduction order):** $\Sigma_{\text{med}} \leftarrow [\,]$.

2: **for** $s = 1$ **to** S **do**

3:     **for** $j = 1$ **to** $K_{\kappa^{(s)}}$ **do**

4:         Append $\langle \kappa^{(s)}, j \rangle$ to Σ_{med}; set $\text{id}_{\text{med}}(\kappa^{(s)}, j)$ to its index.

5:     **end for**

6: **end for**

7: **Glue bins (appended after medoids):** let $M = |\Sigma_{\text{med}}|$.

8: $\text{id}_{\text{bin}}(\theta, b) = M + b$; $\text{id}_{\text{bin}}(\omega, b) = M + B_\theta + b$; $\text{id}_{\text{bin}}(\phi, b) = M + B_\theta + B_\omega + b$.

9: $\Sigma \leftarrow \Sigma_{\text{med}} \cup \{\text{all glue-bin tokens}\}$ (*optional*: add BOS/EOS)

10: **return** $\Sigma, \text{id}_{\text{med}}, \text{id}_{\text{bin}}$

Algorithm 15 BACKBONETOSEQUENCE — tokenize a segmented backbone

---

Require: Protein t_τ with segmentation $\mathcal{P}^{(\tau)} = (\mathcal{M}^{(t_\tau)}_{p_1:q_1}, \ldots, \mathcal{M}^{(t_\tau)}_{p_M:q_M})$; for each $\mathcal{M}^{(t_\tau)}_{p_m:q_m}$ its
  key κ_m and medoid j_m (prototype $\Pi^{(\kappa_m)}_{j_m}$); boundary glue $\Gamma_{q_m} = \{\theta^{CNCA}_{q_m}, \omega_{q_m}, \phi_{q_m+1}\}$ for
  $m = 1{:}M{-}1$; quantizers $Q_\theta, Q_\omega, Q_\phi$; token id maps from Alg. 14.
Ensure: Token sequence $x^{(\tau)} = (x_1, \ldots, x_L) \in \Sigma^L$.
 1: $x^{(\tau)} \leftarrow [\,]$ (optionally prepend BOS/append EOS)
 2: **for** $m = 1$ **to** M **do**
 3:    **Motif:** $x^{(\tau)}.\mathrm{append}\big(\mathrm{id}_{\mathrm{med}}(\kappa_m, j_m)\big)$
 4:    **if** $m < M$ **then**
 5:      **Glue quantize:** $b_\theta \leftarrow Q_\theta(\theta^{CNCA}_{q_m}), \;\; b_\omega \leftarrow Q_\omega(\omega_{q_m}), \;\; b_\phi \leftarrow Q_\phi(\phi_{q_m+1})$
 6:      **Emit (fixed order):** $\quad x^{(\tau)}.\mathrm{append}\big(\mathrm{id}_{\mathrm{bin}}(\theta, b_\theta)\big); \quad x^{(\tau)}.\mathrm{append}\big(\mathrm{id}_{\mathrm{bin}}(\omega, b_\omega)\big);$
   $x^{(\tau)}.\mathrm{append}\big(\mathrm{id}_{\mathrm{bin}}(\phi, b_\phi)\big)$
 7:    **end if**
 8: **end for**
 9: **return** $x^{(\tau)}$

Algorithm 16 RESINITTOKENS — initialize bond–residue codebook and quantize all residues

---

Require: Backbones $\{t^{(1)}, \ldots, t^{(T)}\}$ with lengths $N^{(\tau)}$; targets K_3 (interior bond–residues), K_2
  (terminal bond–residues)
Ensure: Codebooks $\mathcal{A}_3 = \{\Pi^{(3)}_j\}^{K_3}_{j=1}$, $\mathcal{A}_2 = \{\Pi^{(2)}_j\}^{K_2}_{j=1}$; labels $c^{(3)}, c^{(2)}$; backbones with per-
  residue internals set to their prototypes
 1: **Collect occurrences:**

$$\mathcal{S}_3 = \{u \equiv (\tau, i) : 1 \le i < N^{(\tau)}, \; \mathcal{M}^{(t_\tau)}_{i:i} \text{ interior}\}, \quad \mathcal{S}_2 = \{u \equiv (\tau, i) : i = N^{(\tau)}, \; \mathcal{M}^{(t_\tau)}_{i:i} \text{ terminal}\}.$$

 2: **Cluster interiors:** RMSD_PARTITION$(\mathcal{S}_3, K_3) \to$ medoids $\widehat{\mathcal{M}}_3 = \{\widehat{m}^{(3)}_j\}^{K_3}_{j=1}$ and labels $c^{(3)} :$
   $\mathcal{S}_3 \to \{1, \ldots, K_3\}$
 3: **Define interior prototypes:** for $j = 1{:}K_3$, let $u^\star = \widehat{m}^{(3)}_j$ and

$$\Pi^{(3)}_j = \big(\ell^{N-CA}_{i_{u^\star}}, \; \ell^{CA-C}_{i_{u^\star}}, \; \ell^{C-N}_{i_{u^\star}}, \; \theta^{NCAC}_{i_{u^\star}}, \; \theta^{CACN}_{i_{u^\star}}, \; \psi_{i_{u^\star}}, \; \omega_{i_{u^\star}}, \; \phi_{i_{u^\star}}\big)$$

   (*omit undefined terms for a single residue if using a minimal parameterization*).
 4: **Quantize interiors:** for $u = (\tau, i) \in \mathcal{S}_3$ with $j = c^{(3)}(u)$,

$$(\ell, \theta, \psi, \omega, \phi)\big|_{\mathcal{M}^{(t_\tau)}_{i:i}} \leftarrow \Pi^{(3)}_j.$$

 5: **Cluster terminals:** RMSD_PARTITION$(\mathcal{S}_2, K_2) \to$ medoids $\widehat{\mathcal{M}}_2 = \{\widehat{m}^{(2)}_j\}^{K_2}_{j=1}$ and labels
   $c^{(2)} : \mathcal{S}_2 \to \{1, \ldots, K_2\}$
 6: **Define terminal prototypes & quantize:** for $j = 1{:}K_2$, let $u^\star = \widehat{m}^{(2)}_j$ and set the appropriate
   terminal tuple (e.g., $\ell^{N-CA}_i, \; \ell^{CA-C}_i, \; \theta^{NCAC}_i$) as $\Pi^{(2)}_j$; for $u = (\tau, N^{(\tau)})$ with $j = c^{(2)}(u)$,

$$(\ell, \theta)\big|_{\mathcal{M}^{(t_\tau)}_{N^{(\tau)}:N^{(\tau)}}} \leftarrow \Pi^{(2)}_j.$$

 7: **return** $\mathcal{A}_3, \mathcal{A}_2, \; c^{(3)}, c^{(2)}$, and updated backbones

---

Algorithm 17 GLUEOPT — single-boundary IK to absorb one rounding drift

---

Require: Occurrence u with motif $\mathcal{M}_{i_u:k_u}^{(t_u)}$ and medoid $\widehat{m}_{c(u)}$ from RMSD_PARTITION; frames $\{F_i^{\star,(t_u)}\}$ with $F_1^{\star,(t_u)}$ from SEEDTRIAD; weights (w_R, w_t); steps T, step size η

Ensure: $\Gamma_{i_u-1}^{(t_u)}, \widehat{F}_{k_u}^{(t_u)}$

1: **Snap internals:** replace $\mathcal{M}_{i_u:k_u}^{(t_u)}$ by its medoid $\mathcal{M}_{i_{\widehat{m}_{c(u)}}:k_{\widehat{m}_{c(u)}}}^{(t_{\widehat{m}_{c(u)}})}$; set $T_u^{\mathrm{med}} \leftarrow T_{i_{\widehat{m}_{c(u)}}:k_{\widehat{m}_{c(u)}}}^{\mathrm{int}}$

2: **Drift:** $T_u^{\mathrm{occ}} \leftarrow T_{i_u:k_u}^{\mathrm{int}}$; $\Delta T_u \leftarrow T_u^{\mathrm{occ}}(T_u^{\mathrm{med}})^{-1}$

3: **Vars:** $\Gamma_{i_u-1}^{(t_u)} = \{\theta_{i_u-1}^{CNCA}, \omega_{i_u-1}, \varphi_{i_u}\}$ are the *only* optimization variables[4]; init to originals

4: **FK:** keep $F_{i_u-1}^{\star,(t_u)}$ fixed; for any $\Gamma_{i_u-1}^{(t_u)}$,

$$\widehat{F}_{k_u}^{(t_u)} = F_{i_u-1}^{\star,(t_u)} \, \widehat{G}_{i_u-1}^{(t_u)}(\Gamma_{i_u-1}^{(t_u)}) \, T_u^{\mathrm{med}}$$

5: **Loss:**

$$\mathcal{L}_u(\Gamma_{i_u-1}^{(t_u)}) = w_R \big\| \log((\widehat{R}_{k_u}^{(t_u)})^\top R_{k_u}^{\star,(t_u)}) \big\|_2^2 + w_t \big\| \widehat{t}_{k_u}^{(t_u)} - t_{k_u}^{\star,(t_u)} \big\|_2^2$$

6: **Optimize (autodiff):** for $s = 1{:}T$: run FK & evaluate $\mathcal{L}_u$; compute $\nabla_{\Gamma_{i_u-1}^{(t_u)}} \mathcal{L}_u$; update $\Gamma_{i_u-1}^{(t_u)}$ (e.g., Adam, lr η); wrap $\psi, \varphi \in (-\pi, \pi]$, project $\theta^{CNCA} \in (0, \pi)$

7: **return** $\Gamma_{i_u-1}^{(t_u)}, \widehat{F}_{k_u}^{(t_u)}$

Algorithm 18 GLUEOPTALL (WRAPPER) — apply rounding, then call the core global IK over glues

---

Require: Medoids $\widehat{\mathcal{M}}$ and assignments $c(\cdot)$ from RMSD_PARTITION; a set of occurrences $\mathcal{S} = \{u\}$ to round, each $\mathcal{M}_{i_u:k_u}^{(t_u)}$; cached original exit frames for each backbone t (seeded by SEED-TRIAD); histogram bin centers & thresholds for $(\omega, \theta^{CNCA}, \varphi)$; prior weights; loss weights (w_R, w_t).

Ensure: Updated glue angles (snapped to bins) for all boundaries in all affected backbones; recomputed frames $\{\widehat{F}_i^{(t)}\}$.

1: **(Quantize internals)** For each $u \in \mathcal{S}$, replace

$$\mathcal{M}_{i_u:k_u}^{(t_u)} \longleftarrow \mathcal{M}_{i_{\widehat{m}_{c(u)}}:k_{\widehat{m}_{c(u)}}}^{(t_{\widehat{m}_{c(u)}})}$$

by copying the medoid's internal coordinates (hard assignment).

2: **(Ensure targets are cached)** For each backbone t, ensure original exit frames $\{(R_{\mathrm{occ}}^{\star,(t)}[j], t_{\mathrm{occ}}^{\star,(t)}[j])\}_{j=1}^{N^{(t)}-1}$ are available (compute once if missing).

3: **(Global glue optimization)** *Call the core routine* GLUEOPTALL *on all backbones:*

$$\text{GLUEOPTALL}\Big(\{t\}, \text{BinCenters}, \text{Thresholds}, \text{GluePrior}, w_R, w_t\Big),$$

which jointly optimizes every boundary's glue triplet $\Gamma_i = \{\theta_i^{CNCA}, \omega_i, \varphi_{i+1}\}$ via differentiable FK and snaps each angle to the nearest histogram bin.

4: **return** updated glues and frames $\{\widehat{F}_i^{(t)}\}$.

Algorithm 19 BINGEOPAIRS — build the dictionary of geo-pair occurrences (with hierarchy)

Require: For each backbone $t^{(\tau)}$: its current segmentation $\mathcal{P}^{(\tau)} = (\mathcal{M}_{p_1:q_1}^{(t_\tau)}, \ldots, \mathcal{M}_{p_{M_\tau}:q_{M_\tau}}^{(t_\tau)})$ *and*
its merge hierarchy $\mathcal{F}^{(\tau)}$ whose frontier leaves, in order, equal $\mathcal{P}^{(\tau)}$; precomputed boundary-glue quantizers $Q_{\theta^{CNCA}}, Q_\omega, Q_\phi$ (used only at pair boundaries).
Ensure: A *priority-ordered* map $\mathcal{D}$ from keys to occurrence sets, with ordered keys $\pi(\kappa) = (\rho(\kappa), -|\mathcal{O}(\kappa)|, \kappa)$ where $\rho(\kappa) = \mathbf{1}[\kappa \notin \mathrm{dom}(\mathcal{V})]$ indicates if the key already has prototypes.
 1: Initialize an empty ordered map $\mathcal{D}$.
 2: **for** $\tau = 1$ **to** T **do**
 3:    Let $(\mathcal{M}_{p_1:q_1}^{(t_\tau)}, \ldots, \mathcal{M}_{p_{M_\tau}:q_{M_\tau}}^{(t_\tau)})$ be the frontier leaves of $\mathcal{F}^{(\tau)}$ (these equal $\mathcal{P}^{(\tau)}$).
 4:    **for** $j = 1$ **to** $M_\tau - 1$ **do**
 5:       $(\mathcal{L}, \mathcal{R}) \leftarrow (\mathcal{M}_{p_j:q_j}^{(t_\tau)}, \mathcal{M}_{p_{j+1}:q_{j+1}}^{(t_\tau)})$
 6:       $\kappa \leftarrow$ COMPUTEGEOKEY$(\mathcal{L}, \mathcal{R})$ (raw medoid internals inside $\mathcal{L}, \mathcal{R}$; boundary glue quantized by Q)
 7:       Insert the occurrence $(\mathcal{L}, \mathcal{R})$ into $\mathcal{O}(\kappa)$.
 8:    **end for**
 9: **end for**
10: **for** each key κ with nonempty $\mathcal{O}(\kappa)$ **do**
11:    Set $\rho(\kappa) \leftarrow \mathbf{1}[\kappa \notin \mathrm{dom}(\mathcal{V})]$.
12:    Insert $\big((\rho(\kappa), -|\mathcal{O}(\kappa)|, \kappa) \mapsto \mathcal{O}(\kappa)\big)$ into $\mathcal{D}$.
13: **end for**
14: **return** $\mathcal{D}$.

Algorithm 20 COMPUTEGEOKEY — discrete key for an adjacent motif pair

---

Require: Adjacent motifs $\mathcal{L} = \mathcal{M}_{p:q}^{(t)}$, $\mathcal{R} = \mathcal{M}_{q+1:r}^{(t)}$ on backbone t
Ensure: Canonical, hashable key κ for the geo-pair
 1: **Interiors (as stored post-quantization):**

$$\mathrm{Int}(\mathcal{L}) = \Big(\{\ell, \theta, \psi, \omega, \phi\}\big|_{i=p}^q, \{\Gamma_i\}_{i=p}^{q-1}\Big), \quad \mathrm{Int}(\mathcal{R}) = \Big(\{\ell, \theta, \psi, \omega, \phi\}\big|_{i=q+1}^r, \{\Gamma_i\}_{i=q+1}^{r-1}\Big)$$

   (kept unchanged in the key).
 2: **Boundary glue (quantized):**

$$\Gamma_q = (\theta_q^{CNCA}, \omega_q, \phi_{q+1}), \qquad \widetilde{\Gamma}_q = \big(Q_\theta(\theta_q^{CNCA}), Q_\omega(\omega_q), Q_\phi(\phi_{q+1})\big)$$

   ($Q_\bullet$ wrap to a fixed 2π interval before snapping).
 3: **Canonical record & hash:**

$$\mathrm{rec} = \big(\mathrm{Int}(\mathcal{L}), \widetilde{\Gamma}_q, \mathrm{Int}(\mathcal{R})\big), \qquad \kappa \leftarrow \mathrm{HASH}(\mathrm{rec})$$

 4: **return** κ

Algorithm 21 COMPUTE_COORDS — Internal → Cartesian for a bond–residue motif $i{:}j$

Require: Internal geometry for $r = i, \ldots, j$ (bond lengths/angles/dihedrals).
Ensure: $\mathbf{X} \in \mathbb{R}^{3(j-i+1)\times 3}$ for $(N_i, \mathrm{CA}_i, C_i, \ldots, N_j, \mathrm{CA}_j, C_j)$
 1: **Seed residue** i**:** $(N_i, \mathrm{CA}_i, C_i) \leftarrow$ SEEDTRIAD(i)
 2: $\mathcal{C} \leftarrow [N_i, \mathrm{CA}_i, C_i]$
 3: **for** $r = i + 1$ **to** j **do**
 4:    $N_r \leftarrow$ PLACEDIHEDRAL$\big(\mathcal{C}[-3], \mathcal{C}[-2], \mathcal{C}[-1]; \ell_{r-1}^{C-N}, \theta_{r-1}^{CACN}, \psi_{r-1}\big)$; $\mathcal{C}$.append(N_r);
 5:    $\mathrm{CA}_r \leftarrow$ PLACEDIHEDRAL$\big(\mathcal{C}[-3], \mathcal{C}[-2], \mathcal{C}[-1]; \ell_r^{N-CA}, \theta_{r-1}^{CNCA}, \omega_{r-1}\big)$; $\mathcal{C}$.append(CA_r)
 6:    $C_r \leftarrow$ PLACEDIHEDRAL$\big(\mathcal{C}[-3], \mathcal{C}[-2], \mathcal{C}[-1]; \ell_r^{CA-C}, \theta_r^{NCAC}, \varphi_r\big)$; $\mathcal{C}$.append(C_r)
 7: **end for**
 8: $\mathbf{X} \leftarrow [N_i, \mathrm{CA}_i, C_i, \ldots, N_j, \mathrm{CA}_j, C_j]$
 9: **return** $\mathbf{X}$

Algorithm 22 PLACEDIHEDRAL$(a, b, c;\ L,\ \beta,\ \tau)$

1: Right-handed local frame at c:

$$\hat{\mathbf{b}} = \frac{c - b}{\|c - b\|}, \quad \mathbf{n} = \frac{(b - a) \times \hat{\mathbf{b}}}{\|(b - a) \times \hat{\mathbf{b}}\|}, \quad \tilde{\mathbf{n}} = \mathbf{n} \times \hat{\mathbf{b}}.$$

2: Local offset:

$$\mathbf{d} = \left[-L \cos \beta \right] \hat{\mathbf{b}} + \left[L \cos \tau \sin \beta \right] \tilde{\mathbf{n}} + \left[L \sin \tau \sin \beta \right] \mathbf{n}.$$

3: Return $d = c + \mathbf{d}$.

Algorithm 23 SEEDTRIAD(r) — seed triad for residue r

Require: Canonical seed $(N_\star, \mathrm{CA}_\star, C_\star)$; target $L_{CA\text{-}C} = \ell_r^{CA\text{-}C}$, $L_{N\text{-}CA} = \ell_r^{N\text{-}CA}$, and $\theta_{NCAC} = \theta_r^{NCAC}$.

1: Place $\widetilde{\mathrm{CA}}_r$ on the ray from $C_\star$ toward $\mathrm{CA}_\star$ at distance $L_{CA\text{-}C}$.
2: Let $\mathbf{u} = N_\star - \widetilde{\mathrm{CA}}_r$ and $\mathbf{v} = C_\star - \widetilde{\mathrm{CA}}_r$. Rotate $\mathbf{u}$ about axis $\mathbf{u} \times \mathbf{v}$ to achieve angle θ_{NCAC}, then rescale to length $L_{N\text{-}CA}$; translate by $\widetilde{\mathrm{CA}}_r$ to get N_r.
3: Set $C_r \leftarrow C_\star$ and return $(N_r, \widetilde{\mathrm{CA}}_r, C_r)$.